Geomorphic Records along the General Carrera (Chile)–Buenos Aires (Argentina) Glacial Lake (46°-48°S), Climate Inferences, and Glacial Rebound for the Past 7–9ka

Jacques Bourgois, Maria Eugenia Cisternas, Regis Braucher, Didier Bourles, José Frutos

1   **Geomorphic records along the General Carrera (Chile)-Buenos Aires**

2   **(Argentina) glacial lake (46-48°S), climate inferences and glacial rebound**

3   **for the past 7-9 ka**

4

5   [a,b,] [*]Jacques Bourgois,   [c]Maria Eugenia Cisternas, [d]Régis Braucher, [d]Didier Bourlès, [e]Jose

6   Frutos

7

8   [a]Sorbonne Universités, UPMC Univ Paris 06, UMR 7193, Institut des Sciences de la Terre
9   Paris (iSTeP), F-75005, Paris, France. P: 33 (0)1 44 27 59 98; E-mail:
10   jacques.bourgois@upmc.fr
11
12   [b]CNRS, UMR 7193, Paris, France.
13
14   [c]Instituto de Geologia Economica Aplicada (GEA), Universidad de Concepcion, Chile. P: 56
15   4 12 20 48 18; E-mail: mcisternas@udec.cl
16
17   [d]Aix-Marseille Université, CNRS-IRD-Collège de France, UM 34 CEREGE, Technopôle de
18   l'Environnement Arbois-Méditerranée, BP80, 13545 Aix-en-Provence, France. P: 33 (0)4 42
19   97 15 09 ; E-mail: braucher@cerege.fr, P: 33 (0)4 42 97 15 16; E-mail: bourles@cerege.fr
20
21   [(e)]Economic Geologist Consultant, San Juan de Luz 4060, Providencia, Santiago, Chile. P: 56
22   (0)9 89 00 74 00; E-mail: frutosjg@gmail.com
23

24   **Abstract**

25   We present geomorphic, stratigraphic, and chronological data acquired along the General

26   Carrera-Buenos Aires (GCBA) glacial lake located along a major morphological incision

27   across the Andes. Complementing relevant available data, relative chronology of morpho-

28   climatic records together with 18 [10]Be Cosmic Ray Exposure (CRE) ages allow constraining

29   the timing of the Patagonian ice-sheet fluctuations since the LGM. It improves the knowledge

30   of the Patagonia climate evolution in the 46-48°S area, and allows documenting the uplift

31   rates (glacial rebound) for the past ~7-9 ka. The first major ice lobe retreat occurred after 17.3

32   ± 0.6 ka and has likely continued during the ACR from ~12.9 to 14.5 ka. Between ~12.9 ka

33   and ~10.9 ± 1.3 ka, the General Carrera Lake evolved as an endorheic basin. Terraces T4 to

34   T1 (top to bottom) have recorded abrupt lake regressions likely controlled by rainfall deficit.

35   They have accumulated in the time interval ~17.3-12.3 ka (maximum limits). Two glacial re-

36   advances at ~10.9 ± 1.3 and ~7.9 ± 1.1 ka marked a major climate change that led the lake to

37   be ice-dammed again. A major transgression occurred subsequently that have flooded the

38   previously accumulated terraces. Since then, a pervasive regression has steered the GCBA

39 Lake to the situation at Present. The highest shoreline of the transgression is used as a passive
40 marker in order to quantify the magnitude and character of the regional deformation. At
41 72°30' W, the GCBA Lake area uplifted (glacial rebound) at a rate between 15 to 33.5 mm.yr⁻
42 ⁻¹ during the past ~7.9 ± 1.1 ka. We infer that the high uplift rate mainly originates from the
43 North Patagonian icefield ice loss.

44

45 **Keywords:** Patagonia, General Carrera Lake (Chile), Buenos Aires Lake (Argentina),
46 Morphology, Stratigraphy, Chronology, Cosmic Ray Exposure ages, Last Glacial Maximum,
47 Holocene, Climate inferences, Isostatic rebound, Slab window.

48

49 **1. Introduction**

50

51   The N-S trending Andes separating the Pacific Ocean to the West from the foreland
52 lowlands to the East dominate the topography of Patagonia. An elongated ice sheet, the
53 Patagonian ice sheet (Fig. 1), extending over 1800 km between 38° and 56°S covered the high
54 relief of this major mountain belt (Kaplan et al., 2004; Sugden et al., 2002; Lowell et al.,
55 1995; Hulton et al., 1994) during the Last Glacial Maximum (LGM) at ~19-29 ka (Boex et al.,
56 2013; Hein et al., 2009; Douglass et al., 2006; Kaplan et al., 2004; Singer et al., 2000;
57 Fleming et al., 1998). The North and the South Patagonian icefields (NPI and SPI,
58 respectively) are today restricted remnants of the maximum glacier extent. At Present, these
59 Patagonian icefields are the largest glaciers in the southern hemisphere outside of Antarctica.
60   At 46-48°S the GCBA Lake is the trace of a major ice lobe that originated from the NPI
61 (Fig. 2). Moraine markings provide record of ice retreat since the LGM **(**Glasser et al., 2012;
62 Kaplan et al., 2011; Moreno et al., 2009; Kaplan et al., 2004; Wenzens, 1999; Clapperton,
63 1997; Marden and Clapperton, 1995; Markgraf et al., 1992; Mercer, 1982). At Present the
64 GCBA Lake flows to the Pacific Ocean bypassing the Andes crest line at ~2000-4000 m
65 through the Rio Baker. Because a thick ice sheet covered the Andes during maximum ice
66 extent melt water had to stream eastward through the Rio Deseado that drained the Andes to
67 the Atlantic Ocean during the LGM and part of the subsequent deglaciation. In this study we
68 investigate the ice retreat history and water level fluctuations along the GCBA Lake for the
69 past ~27-29 ka with special reference for the past ~15-17 ka following the last main ice lobe
70 development. We use the in-situ produced ¹⁰Be cosmogenic nuclide to determine the CRE
71 ages of samples from boulders located at moraine crests, drop-stones on terraces, and
72 preserved glacial polish on bedrock. The CRE ages of dropstones resting on strandlines and

73 terraces allowed us to reconstruct confidently the GCBA Lake evolution, outlet routing, and

74 history during the LGIT and the Holocene that complement the pioneer studies by Bell (2008)

75 and Turner et al. (2005). The evolution of the GCBA Lake area provides constraints on the

76 vertical isostatic adjustment (i.e. rebound) driven by ice decay and ice volume loss for the

77 past 7-9 ka.

78

79 **2. Background**

80

81 2.1. Geologic setting

82

83   The studied area (45-48°S) is located at the latitude of the Chile triple junction area (Fig. 1)

84 where the Antarctica, the Nazca, and the South America plates meet (Bourgois et al. 2000;

85 Behrmann et al., 1992; Leslie, 1986; Cande and Leslie, 1986). At 46°09'S, the active

86 spreading center at the Antarctic-Nazca plate boundary –i.e. the Chile ridge– is being

87 subducted beneath the South America continental margin. When a spreading ridge intersects a

88 subduction zone, the diverging oceanic plate edges become surrounded by hot mantle, a slab

89 window develops at depth (Dickinson and Snyder, 1979; DeLong et al., 1978). At the studied

90 area, the Patagonian slab window extends beneath the GCBA Lake area at depth (Russo et al.,

91 2012; Breitsprecher and Thorkelson, 2009; Bourgois and Michaud, 2002). The GCBA Lake

92 area is slab-free (Gorring and Kay, 2001; Gorring et al., 1997). Plio-Pleistocene basalts that

93 erupted along this area at the Meseta del Lago Buenos-Aires provide evidence for

94 asthenosphere-lithosphere interaction during slab window development (Orihashi et al., 2013;

95 Guivel et al., 2006; Gorring et al., 2003; Gorring and Kay, 2001). This situation has an impact

96 on the mechanical strength properties of the Patagonia lithosphere and upper mantle that in

97 turn must induce a signature on the rate of vertical crustal motion (rebound) associated with

98 ice mass loss.

99   The Andean batholith of Cretaceous to Lower Miocene age (SERNAGEOMIN, 2002) is a

100 major rock unit of the Patagonia Andes. Along the studied transect, it extends from the

101 Bertrand Lake to the east to the Pacific coastline to the west intruding metamorphic

102 complexes over a distance of more than 100 km. The major component of the moraines and

103 drop-stones from the GCBA ice lobe are granitic rock from the Patagonian batholith.

104

105 2.2. Paleoclimatic background

106

107   The 3 to 4 km high Patagonian Andes form a prominent topographic barrier to the

108   Westerlies atmospheric circulation in the southern hemisphere and cause one of the most

109   pronounced orographic rain shadow on Earth. Between 46° and 49°S rainfall along the Pacific

110   western slopes is >3000 mm.yr^{-1}, ~10 times higher than along the eastern side of the

111   Argentina Andean foreland (Hoffman, 1975). The Pacific Ocean to the west, together with the

112   Andean Cordillera with peaks rising above 3000 m and the dry steppes of Argentina in the

113   rain shadow of the Andes to the east control the climate of Patagonia. The cool temperate belt

114   extends south of 42°S (Miller, 1976) while the Westerlies and precipitation reach a maximum

115   at around 50°S where the mean annual precipitation may exceed 5000 mm at sea level.

116   Precipitation totals decrease sharply northward from 2000 mm at 40°S to <150 mm at 30°S

117   (Hoffman, 1975). Numerical modeling aiming to reconstruct the climate of Patagonia during

118   the LGM (Hulton et al., 1994) shows a northward migration of precipitation belt of ~ 5° (Fig.

119   1) with a decrease of the annual precipitation totals at 50°S and an increase at 40°S, the

120   Westerlies reaching a maximum at 45°S. The topographic barrier of the Andes is expected to

121   influence the atmospheric circulation similarly during both glacial and interglacial periods.

122

123   2.3. Timing of ice retreat

124

125   In the GCBA Lake area, the maximum extent of the LGM ice lobe occurred between ~25

126   and 29 ka (Boex et al., 2013; Hein et al., 2010). This is in agreement with the glacial

127   maximum at 26-27 ka B.P. identified at the Lago Llanquihue piedmont lobe (Lowell et al.,

128   1995) located several hundreds of km to the north. The LGM and the subsequent retreat of the

129   GCBA ice lobe is marked by a large moraine system located at 150-200 km east of the NPI

130   (Singer et al., 2000; Kaplan et al., 2004; Douglass et al., 2006; Hein et al., 2009). Based on

131   paired ^{10}Be and ^{26}Al ages, Kaplan et al. (2004) have first identified the youngest

132   Fenix/Menucos moraine complex at the Perito Moreno outlet area with ages ranging from

133   22.9 ± 1.3 to 15.1 ± 0.5 ka. Subsequently, the in-situ produced ^{10}Be production rate, ^{10}Be half-

134   life and muonic production parameters have been dramatically revised (Blard et al., 2013;

135   Kelly et al., 2014; Braucher et al., 2011; Chmeleff et al., 2010, Korschinek et al., 2010). This

136   implies that all CRE ages published before 2010 are systematically underestimated by at least

137   28% considering in addition that the ^{10}Be half-life they used is ~9% higher than the recently

138   re-evaluated one. Kaplan et al. (2011) have re-calculated the Fenix I to V and the Menucos

moraine ages using updated parameters close to those accepted at present. They have documented the following mid point ages for the Menucos and Fenix I to V terminal moraines: Menucos (17.3 ± 0.6 ka), Fenix I (18.5 ± 0.8 ka), Fenix II (19.8 ± 0.6 ka), Fenix III (21.8 ± 0.7 ka), Fenix IV (26.3 ± 0.9 ka), Fenix V (25.7 ± 0.9 ka). Therefore, the timing of the onset of massive deglaciation has occurred between 16.7 and 17.8 ka, after the last re-advance or still stand of the ice lobe recorded by the Menucos Moraine. However, this re-calculated [10]Be ages from Kaplan (2011) conflict the previous description by Kaplan et al. (2004). Indeed they have shown that the youngest Menucos moraine is overlying lake sediment dated at 15.5 ± 0.5 cal ka (AMS radiocarbon age). Consequently, the age of the last major ice re-advance must be younger than 15 to 16 ka. This opens the question of the attribution of this moraine to the Menucos moraine. A re-advance of the GCBA ice lobe that would be younger than the Menucos moraine may exist in the Perito Moreno outlet area. Recently, Boex et al. (2013) have presented a reconstruction of the Patagonia ice-sheet evolution from the LGM. They considered that the ice-sheet profile has remained extensive and close to its LGM extent until ~19 ka. Rapid ice-sheet thinning initiated at 18.1 ka reaching its present dimension at 15.5 ka. The outcomes from Boex et al. (2013) are conflicting with those from Kaplan et al. (2011 and 2004) with a gap of ~150 km in ice extent during the same time window, along the same area. Also, Boex et al. (2013) claim that no substantial ice re-advance has occurred during the Antarctic Cold Reversal (ACR) and the Younger Dryas (YD).

To document paleoclimat changes during the LGIT, a palynological record from the Guanaco Lake (Torres del Paine area) was developed (Moreno et al., 2009). The obtained record documents dominance of pre-Andean herbs and shrubs between 11.4 and 12.5 ka and a rapid increase in *Nothofagus* ca. 12.3 ka that document the onset of massive ice recession at ca. 12.6 ka at about 50°S.

In the study area, published data reveal contradictions. In this work, the accepted assumptions and ages are as follow: (1) a major re-advance of the GCBA ice lobe occurred at 15 to 16 ka, the major ice recession has to occur subsequently; (2) ages for the YD (11.5 to 12.8 ka) and the Antarctic Cold Reversal (ACR, 12.9 to 14.5 ka) are those from Jomelli et al. (2014) that use the most recent updated production rates for cosmogenic [10]Be and [3]He; (3) the onset of massive ice recession occurred at ~12.6 ka.

2.4. GCBA Lake evolution

172   The E-W trending GCBA Lake is 585 m deep (Murdie et al., 1999) and 130 km long

173   extending ~ 55 km eastward across the Andean foreland. To the west, the Rio Baker —i.e. the

174   outlet of the GCBA Lake, water level at 201 m— streams between the disconnected NPI and

175   SPI (3-4 km in elevation), until reaching the Pacific. At Present the drainage divide (392 m at

176   Perito Moreno) is located along the Fenix moraine system at the eastern ends of the GCBA

177   Lake. During the LGM a continuous ice sheet blocked the route to the Pacific causing

178   meltwater from the GCBA ice lobe to drain to the Atlantic. After 15-16 ka, deglaciation

179   results in a drainage diversion as the ice disintegrated in the Andes (Hein et al., 2010; Bell,

180   2008; Turner et al., 2005; Bourgois et al., 2000; Mercer, 1976; Caldenius, 1932). During the

181   LGIT, cold events such as the ACR, the Younger Dryas, and the subsequent 8.2 ka Cold

182   Event, major glaciers including those from tributaries of the Rio Baker potentially dammed

183   the water outflow to the Pacific (Boex et al., 2013; Hein et al., 2010; Bell, 2008; Glasser et

184   al., 2005; Turner et al., 2005) resulting in ice-dammed paleolake formation. Geologic

185   evidence indicates the presence of such paleolakes at heights ranging from about 100 m to

186   about 330 m above the present-day elevation of the GCBA Lake. Evidence includes

187   paleoshorelines, beaches, terraces, raised deltas, and lake sediments (Bell, 2008; Douglass et

188   al., 2005; Turner et al., 2005; Wenzens, 2005; Caldenius, 1932).

189   Turner et al. (2005) have described the GCBA Lake fan-deltas and terraces through the

190   concept of the "United Lake", which closely associates the GCBA (201 m in elevation at

191   Present) and the Cochrane-Pueyrredon (CP, 152 m in elevation at Present, Fig.1) Lakes

192   evolution. The routing of the "United Lake" water to the Atlantic occurred through the Rio

193   Deseado. Using 16 ages, 15 of them being located outside the GCBA Lake, they reported the

194   development of two paleolake shorelines along the GCBA Lake. Mollusc shells sampled

195   along a terrace (315 m in elevation, lower paleolake shoreline) located at the Chile Chico

196   Mirador have provided a cosmogenic calibrated age of 13.5 ± 0.2 ka. Subsequently, Hein et

197   al. (2010) developed a model based on the "United Lake" concept. They have proposed an

198   evolution through two steps, the Upper United-paleolake (fan delta at 370-400 m in elevation)

199   and the Lower United-paleolake (fan delta at 300-270 m in elevation) steps, both occurring in

200   the time interval 15-16.5 ka.

201   From a detail study of the Rio de Las Dunas area (GCBA Lake), Bell (2008) has conducted

202   a focused analysis on the paleolake levels. Bell (2008) identifies a series of seven raised

203   lacustrine braided deltas at elevations ranging from 100 to 450 m above Lago General Carrera

204   i.e. ~300 to 650 m amsl. The deltas were formed by the punctuated drainage of a paleolake

205   called the "Predecessor Lake" —i.e. the two GCBA-CP connected lakes—. Breaking of ice

206   dam would have caused the ''Predecessor Lake'' to drop abruptly by 30 to 150 m, which was

207   followed by periods of stability. A volcanic ash layer covering the Bell's ''Delta 2''—i.e.

208   equivalent to the Lower United-paleolake of Turner et al. (2005)— was ascribed to a 6.7 ka

209   BP eruption of Volcan Hudson (Bell, 2008). If this interpretation is correct, it provides a

210   benchmark age for the Deltas 2 and 1, which are older and younger than 6.7 ka, respectively.

211   Also, Bell (2008) suggests that the Delta 1 was still in existence at this time in the Holocene.

212   Bell (2008) considers that the punctuated drainage of the ''Predecessor Lake'' as recorded by

213   Deltas 1 to 7 began at ~13 ka ago.

214

215   **3. Methods**

216

217   3.1. Geomorphic imprints

218

219   Three main geomorphic features have recorded the morpho-climatic and tectonic evolution

220   of the studied area. These signatures include moraines at the glacial lobe terminations, fan-

221   deltas built by stream-transported sediments to the GCBA Lake, and a dense flight of

222   strandlines. The strandline sequence documented throughout the GCBA Lake area exhibits a

223   pervasive signature. Regarding the direct action of glaciers, terminal moraines have mainly

224   been sampled east of the GCBA Lake. These moraines have recorded major stages of ice lobe

225   re-advances and related paleo-environmental conditions from the LGM to the ACR.

226   At Present, fan deltas or terraces (Fig. 3) are especially developed along the General

227   Carrera Lake (Chile). Bell (2008) and Turner et al. (2005) have described the GCBA Lake

228   fan-deltas and terraces through the concept of the "Predecessor Lake" and the "United Lake"

229   concepts (see section 2.4.), respectively. Because no age and elevation correlations for fan

230   deltas and terraces of the GCBA and CP Lakes is consistently documented, the present work

231   proposes direct elevation measurements and ages for the GCBA Lake fan deltas.

232   As soon as the water of a stream encounters the standing water of a lake, speed drops

233   rapidly, which leads to the development of a fan-delta from load deposit. An evolving fan-

234   delta is recording the evolution of the lake level through time. Also, the accumulated

235   sediments display evidences of highly variable currents and changes of facies. The braid

236   deltas built into the GCBA Lake display topset, foreset, and bottom layers showing a typical

237   Gilbert Delta organization (Fig. 3D). These geomorphic imprints were described in great

238   details by Bell (2008). Between 201 m —the lake level elevation at Present— and ~ 530 m,

239 the northern and the southern banks of the General Carrera Lake exhibit five main levels, T4

240 to T0 of such fan deltas or terraces (Fig. 3A, B, C, E, and F). Based on a precise mapping of

241 the Rio de Las Dunas area (Bell, 2008), terraces were labeled 7 to 1 from top to bottom.

242 Terraces T4, T3, T2, T1, T0 (top to bottom) ientified in this work match the Bell's terraces 5,

243 4, 3, 2 and 1, respectively. The Bell's terraces 7 and 6 are considered as river terraces in this

244 work. Another major record of the evolution of the lake water level is the strandline

245 sequences underline by notches and wave-cut terraces (Fig. 4A to D). The major terraces

246 identified all around the GCBA Lake connect laterally to strongly notched strandlines. These

247 sequential records, including fan deltas and strandlines, have left in the landscape a strong

248 imprint that underlines the main water level stages. Frequently, a tempestite barrier (Fig. 4A)

249 underlines the coastline at Present. The tempestite records were identified not only along

250 beaches (Fig. 4B) but also at the fan delta front (Fig. 4A) along the shoreline documenting the

251 recent water level lake evolution. The morphologic analysis of the older terraces —i.e. old

252 fan-deltas— shows that such tempestite records exist along the paleo-shorelines. The terraces

253 of the GCBA Lake area exhibit isolated erratic boulders (dropstones) left on terraces (Fig. 5A

254 to D). The dropstone emplacement that post-dates the terrace accumulation allows

255 constraining the lake level evolution, and age during the GCBA ice lobe retreat during the

256 LGIT. The above listed morphologic features and age are used to disentangle the chronology

257 of the GCBA Lake evolution. However, the lake size, the evolution of the potential outlets,

258 and the glacial isostatic rebound make the approach difficult.

259

260 ## 3.2. Sampling procedure and method

261

262 Sampling sites (Fig. 2) are located along the GCBA Lake between 70°30' and 73°50'W,

263 from the eastern foreland of the Andes to the Rio Baker River outlet. All the dated samples

264 but the glacial polish (sample 25, Table 1) originated from granite boulders comprising from

265 15 to 30% quartz. The local geological background consists in a metamorphic basement

266 covered by volcanic and sedimentary rocks that differ from the sampled blocks. The sampled

267 blocks originated from the Patagonian batholith located 50 to 200 km west from their current

268 location. The GCBA ice lobe and icebergs originating from the NPI during the subsequent pro

269 glacial phases of the lake transported them. Our sampling selection strategy has been

270 established to minimize the effects of pre-exposure prior to exposition and of denudation

271 following deposition. Samples were collected by hand with hammer and chisel from the tops

272   of boulders as close to the center of the upper surface as away from the edges as possible.
273   Preference was given to large —i.e. more than 1.5 m in diameter—, flat topped and stable
274   boulders. Only the top 2 to 5 cm of the selected boulders was sampled. The location (Fig. 2),
275   the age (Table 1) and elevation (Table 2) of each boulder and morphologic features were
276   surveyed using two TRIMBLE 4600 LS receivers in association with a hand-held global
277   positioning system (GPS) for lateral correlation. The vertical location of the upper part of
278   terraces and paleo-shoreline locations are the main error source. The accuracy of the field
279   leveling carried out is estimated to be at worst ± 5 m. Elevation was further controlled
280   plotting the sample locations on topographic maps. The estimated horizontal accuracy is
281   better than 3-4 m.

282

283   3.3. Cosmogenic surface exposure dating

284

285   CRE dating is based on the quantification of the cosmogenic nuclide content accumulated
286   in a rock exposed at the surface to cosmic rays. This high-energy cosmic radiation induces a
287   nuclear reaction when penetrating Earth's environment (Lal, 1991 a and b). Energetic
288   particles interact with target atoms to produce cosmogenic nuclides. Eighteen samples (Fig. 2,
289   Table 1) have been collected from key sites. Quartz was isolated and purified from the
290   atmospheric ^{10}Be following the standard method (Merchel and Herpers, 1999; Brown et al.,
291   1992). After dissolution in Suprapur HF, the resulting solution was spiked with 300 μg of ^{9}Be
292   carrier (Brown et al., 1991). Beryllium was extracted (Brown et al., 1992; Bourlès, 1988), and
293   cosmogenic ^{10}Be measurements were performed with the AMS Tandetron facility (Gif-sur-
294   Yvette, France) (Raisbeck et al., 1987, 1994). The measured ^{10}Be/^{9}Be ratios were corrected
295   for procedural blanks and calibrated against the National Institute of Standards and
296   Technology standard reference material 4325 by using an assigned value of $2.79 \pm 0.03 \times 10^{-11}$
297   and a ^{10}Be half-life of $1.387 \pm 0.012 \times 10^{6}$ years (Korschinek et al., 2010; Chmeleff et al.,
298   2010). Analytical uncertainties (reported as 1σ) include uncertainties associated with AMS
299   counting statistics, procedural blank measurements (^{10}Be/^{9}Be = $4.372 \pm 2.524 \times 10^{-15}$) and the
300   AMS internal error (3%). A sea level, high-latitude (SLHL) spallation production of $3.67 \pm$
301   0.17 at.g^{-1}.yr^{-1} calibrated against ^{3}He in the Tropical Andes (Blard et al., 2013) was used and
302   scaled for latitude (Stone, 2000) and elevation. The contribution of muons to the production
303   rate was calculated using the physical parameters recently re-evaluated by Braucher et al.
304   (2011). Because it uses updated physical parameter, the ^{10}Be production rate used in this work

305 is more accurate as compared to that at 3.71 ± 0.11 at.g^{-1}.yr^{-1} proposed by Kaplan et al.

306 (2011). However, the ^{10}Be production rate calculated by Kaplan et al. (2011) in an area

307 located few hundreds of km south of the studied area overlaps that retained in this work.

308 Therefore, no re-calculation is done regarding the ages provided by Kaplan et al. (2011,

309 supplementary material) for the Menucos and Fenix moraines.

310 Because the concentration of in situ produced cosmogenic nuclides depends both on the

311 exposure duration to cosmic rays and on the denudation rate, CRE ages can be calculated only

312 if the relevant denudation rate is known or can be neglected. All minimum CRE ages

313 presented (Table 1) are calculated neglecting denudation, which is justified in our case for

314 most of the discussed samples considering the maximum denudation rates calculated from the

315 samples having reached steady-state (0.049± 0.02 and 1.31 ± 0.16 m/Ma for samples 4 and 17

316 (Table1), respectively and the short time interval investigated that extends at most over the

317 last 40 ka. Vegetation is limited to small shrubs and historical snow accumulation has been

318 thin and short-lived in this semi-arid area (Garreaud et al., 2013). Moreover, climate models

319 suggest that aridity increased during colder periods (Hulton et al. 2002).

320

321 **4. Results**

322

323 4.1. Buenos Aires Lake area

324

325 Two samples (15 and 69, Fig. 6 and 7) were collected along the Menucos and the Fenix I

326 moraine crests. The ^{10}Be analyses (Table 1) yield to minimum ages of 20.5 ± 8.4 and 20.2 ±

327 2.6 ka, respectively. Although imprecise, these values are remarkably similar.

328 Between the current lake level at 201 m and 415 ± 5 m elevation, the Buenos Aires Lake

329 northern rim exhibits a pervasive flight of strandlines (Fig. 8). These regressive parallel

330 strandlines have recorded the complex lake level evolution through time, as it was free of ice.

331 Above 415 ± 5 m elevation, the shore area exhibits several steps characterized by flat parallel

332 strips bounded lakeward by steep side. The flat strips, which exhibit a braided pattern of

333 meander loop, are outwash plains covered by well-rounded conglomerates. The arcuated steep

334 side follows the inner side of the arcuated ridges previously constructed during moraine

335 accumulation. The essential factors for braiding are bed-load sediment transport and laterally

336 unconstrained free-surface flow, conditions that characterize the lateral evolution of a

337 retreating ice lobe. The arcuated moraine succession controls the subsequent evolution of

braided pattern strips. The arcuated moraine ridges have recorded re-advance or still-stand of ice lobe during cold episodes whereas braided pattern evolved subsequently during ice lobe retreat during warmer episodes. Towards the lake, the morphologic signature evolves abruptly to an area characterized by parallel regressive strandlines. In this study, we consider that the Buenos Aires Lake began to be free of ice after the Menucos glacial event. Since then, the evolution to the free-of-ice situation occurred during the ACR (see previous section). Subsequently, the lake water level was fluctuating between elevations ranging from 415 ± 5 to 201 m, mainly controlled by the Bertrand/Baker spillway and rainfall. Along the northern rim of the lake the arcuated moraine pattern controlled the stream drainage. At Present, the Rio Fenix Grande is streaming eastward following the pre-existing moraine/braided pattern morphology.

4.2. Chile Chico area

Sample 23 (Fig. 7) was collected along a perched lateral moraine located west of Chile Chico at ~1116 m amsl. Its ^{10}Be concentration yields to a minimum CRE age of 34.2 ± 10.4 ka (Table 1). The moraine lies on a flat area at less than 10-15 m away from the slope break along the sub-vertical flank of the main U-shaped glacial valley —i.e. the ice edge at the time accumulation of the lateral moraine during the ice growth optimum during the LGM–. Because the GCBA Lake at Present is more than 400 m deep (Murdie et al., 1999), the estimated thickness of ice along the GCBA lobe at the longitude of sample 23 was ~1.5 to 1.7 km during the LGM.

Coupled climate/ice sheet models were developed in order to simulate the inception and growth of the Patagonia ice sheet (Klemann et al., 2007; Sugden et al., 2002; Ivins and James 1999; Hulton and Sugden, 1997). These models simulate the altitude evolution of the snowline through time. The equilibrium-line altitude (ELA) or snowline (Bakke and Nesje, 2011) is the average elevation of the zone where snow accumulation equals ice ablation over a one-year period. Although the ELA is determined by local weather conditions, it is a good proxi of regional climate conditions because glacier mass-balance fluctuations are correlated over distances of ~500 km. At the local and regional scale of the NPI, the ELA position allowed estimating the ice area change (Rivera et al., 2007; Aniya et al., 1996). While the Present ELA position can be determined without major difficulties, collecting relevant data for reconstructing past ice cap evolution remains challenging. Although sometimes

371   questioned, lateral moraines are regarded as reflecting the corresponding ELA since lateral

372   moraines are considered to deposit only in the ablation zone below the ELA. Considered as

373   relevant for lengthy ice lobe, this widely accepted method might provide confident

374   information along the GCBA glacial lake.

375   Therefore sample 23 provides an estimate for the ELA during the LGM. At that time the

376   ELA was at ~1100 m above sea level (no rebound correction), an elevation similar to that

377   proposed for the Chilean Lakes region during the LGM (Porter, 1981). At Present, the ELA

378   along the eastern side of NPI is 1350 m (Aniya, 1988; Casassa, 1987) —i.e. ~250 m

379   (minimum value) higher than during the LGM—.

380

381   4.3. Fachinal area

382

383   Douglass et al. (2005) have studied in great detail the Fachinal area (Fig. 2 for location). At

384   the outlet of the Rio Aviles they have identified two different moraines documenting two ice

385   lobe advances during the Holocene recorded by an Outer and an Inner moraines with ages at

386   8.5 ± 0.7 ka and 6.2 ± 0.8 ka, respectively. These two moraines provide constraint for age

387   accumulation of the underlying T1 terrace, which must be older than the older moraine. In

388   this specific area, the T1 terrace is 314 to 293 m in elevation. Two km northeast of Fachinal,

389   along the northern rim of the General Carrera Lake is the Rio Avellano fan-complex and

390   terraces. At this site, the T0 and T1 terraces exhibit elevations similar to those of Fachinal.

391   Unlike the Fachinal area, the Rio Avellano outlet area shows the development of a T2 terrace

392   with elevation ranging from 391 to 413 m.

393   Because the basic work by Douglass et al. (2005) is a key point not only in itself but also

394   in placing a major step in the climate and geomorphic evolution of the GCBA Lake area, we

395   have re-calculated the Fachinal moraine ages using updated parameters (see sections 2.3 and

396   3.3). The new proposed ages are 10.9 ± 1.3 and 7.9 ± 1.1 ka for the Outer and the Inner

397   moraines, respectively (Fig. 6). Therefore the T1 terrace accumulated before 10.9 ± 1.3 ka.

398

399   4.4. Rio de Las Dunas, Rio Las Horquetas and Rio Los Maitenes area

400

401   Between 201 and 528 m in elevation, the outlet areas of the Rio de Las Dunas, Rio Las

402   Horquetas and Rio Los Maitenes exhibit five major terraces, T0 to T4 from base to top (Fig.

403   9). This area was described in details by Bell (2008). The most recent T0 terrace, still

404   evolving as a fan-delta at Present, exhibits elevation ranging from 201 to 228 m. At Rio de

405   Las Dunas outlet, the T0 terrace protruding northward toward the lake connects eastward to a

406   sequence of 12-15 strandlines —i.e. paleoshore lines—, which developed between 201 and

407   211 m along a small embayment (Y1, Fig. 4 C). One to two meters high tempestite barriers

408   underline the most prominent strandlines. As the lake level drop down, the fan-delta —i.e. the

409   so-called T0 terrace— and laterally connected strandlines develop. The association between

410   sediment accumulation at fan-delta and regressive strandlines strongly suggests that no major

411   rupture in the lake level evolution have occurred during these two coeval morphogenic

412   processes. Two potential factors, including decline in precipitation and bedrock incision at the

413   Rio Bertrand outlet spillway, controlled the lake level drop from 211 to 201 m. Because ice

414   damming occurred along the GCBA Lake spillway, during T1 to T4 terraces accumulation,

415   we infer that the climate —i.e. rainfall deficit— is also responsible for the lake level

416   variations during the time period from the ACR to 10.9 ± 1.3 ka.

417   The elevation of the T1 terrace ranges from 302 to 347 m. This main terrace (Fig. 9 A and

418   B) shows a major development along the General Carrera Lake. Due to the fact that the

419   terrace (Fig. 3F) exhibits deeply notched strandline in its along-shore prolongation, especially

420   in the Pto Guadal area. We infer that it develops during a fairly long time period of stable

421   climate conditions. The T1 terrace cliff exhibits a deep incised valley (point X, Fig. 9 A and

422   B) in which 65 m of sediment accumulated after incision. Because the T0 terrace

423   accumulation post-dates the infill of the valley at point X, a transgression phase has occurred

424   between the T0 and T1 terraces accumulation. South of the Rio de Las Dunas mouth, the T1

425   terrace cliff (point Y3, Fig. 10) exhibits a dense flight of strandlines (point Y3, Fig. 4 C) with

426   a signature similar to those left from tempestites described at the embayment shown at Figure

427   4 C (see above). As documented at point X (Fig. 9 A and B), lake reoccupation occurred with

428   water level rising to the top of the T1 terrace cliff, at least.

429   The T2 terrace is 432 to 468 m in elevation. Along the eastern bank of the Rio de Las

430   Dunas a major flight of strandlines has left a pervasive imprint on the T2 terrace that connects

431   upslope to the area occupied by the T3 terrace. The cliff bounding the T3 terrace downslope is

432   partly removed by subsequent lake reoccupation and associated shoreline erosion. The T2

433   terrace connects southwestward to a deeply notched strandline (Fig. 3 F). The sample 59 from

434   a dropstone lying on the strandline yields a minimum CRE age of 15.0 ± 1.8 ka (Table 1) that

435   constrains the minimum T2 terrace age. The T3 and T4 terraces are 472 to 495 and 499 to 528

436   m in elevation, respectively. As opposed to the lower terraces —i.e. T0 and T1— described

437   above, the T3 and T4 terraces exist only in the Rio de Las Dunas and Rio de Los Maitenes

embayment area. This area exposed to prevailing wind direction exhibits a large amount of dropstones resulting from drifting of icebergs toward this trapping zone. We infer that the T3 and T4 terraces accumulated in an ice-wall lake environment. A large ice lobe was still flowing along the General Carrera Lake at that time. Five dropstones were sampled in this area. The 10 x 6 m granite block (sample 31, Fig. 5 B) on top the T3 terrace (location Fig. 9 B) yields a minimum CRE age of 16.5 ± 4.1 ka (Table 1). Two dropstones, samples 61 and 71 on top of the T4 terrace yield minimum CRE ages of 15.2 ± 3.7 and 18.8 ± 3.9 ka, respectively. To the southwest, in the prolongation of the T4 terrace, sample 57 (Fig. 9 B, Table 1) from a dropstone (Fig. 5 D) located few meters below the uppermost strandline identified along the General Carrera Lake, yields a minimum age of 18.5 ± 3.7 ka. Terraces T3 and T4 exhibit extensive flights of strandlines extending from ~ 527 m in elevation in the area of Rio de Las Dunas to less than 325 m east of Rio Los Maitenes (Fig. 9 B). The imprint of each single strandline and their association as flight exhibits a signature similar to the tempestite flights identified along T0, T1, and T2 terraces (see above). These morpho-climatic imprints document a major phase of transgression, up to the T4 terrace, followed by a retreat of water as recorded across terraces T4 to T1. The sample 73 (Fig. 4 D, 9 B) collected on top the upper tempestite strandline, which notches the T4 terrace at about 521 m elevation, yields a minimum CRE age at 9.9 ± 2.5 ka, significantly younger than dropstones sampled on top T3 and T4 terraces.

4.5. Rio Müller area

The Rio Müller (Fig. 11) is located north of the General Carrera Lake. The lake shoreline east of Bahia Murta (Fig. 2) and its eastward prolongation towards the outlet of the Rio Müller display a pervasive development of terraces T0, T1 and T2 with elevation ranging from 201 to 227, 302 to 334, and 413 to 448 m, respectively. These elevations are consistent to those recorded south of the lake at the same longitude. As at other locations (Fig. 3 D), the Rio Müller outlet area exhibits along the norhern rim of the lake an incision of the T1 and T2 terraces (Fig. 11 B, C) that deeply involves the metamorphic basement rock. Elevation measurements at the surveyed area (Fig. 11 A, B, C) have documented a ~94 m incision (Fig. 11 D) occurring after the T1 and T2 terrace accumulation. Because ~102 m of basement incision occurred after deposition of the T1 terrace accumulation at the Rio El Salto area (Fig. 3 D), we infer a similar situation at the Rio Müller. At this site, most of basement incision is

471   postdating the accumulation of the T1 terrace. As exemplified at Pto Ingeniero Ibañez and Rio

472   de Los Maitenes areas (Fig. 7 and 9, respectively) the basement incision identified at different

473   sites along the General Carrera Lake mainly occurred after the accumulation of the T1 terrace.

474

475   ## 4.6. Western outlet area

476

477   At Present time, the General Carrera Lake flows to the Pacific Ocean through the Lago

478   Bertrand, which connects downstream to the Rio Baker. This simple draining route shows a

479   complex evolution through time (Glasser et al., 2012) involving the Lago Negro, the Lago

480   Bertrand, the Rio Bertrand, the Lago Plomo and the Rio Baker spillways (Fig. 12 and 13).

481   At the El Martillo area (Fig. 12 A, B), the General Carrera Lake is actively outflowing

482   westward to the Lago Bertrand. The channel connecting the General Carrera Lake to the Lago

483   Bertrand erodes ~100 m of the basement rock underlying a moraine ridge cropping out at 300

484   to 450 m elevation. Samples 45 and 49 from the moraine (Fig. 12 B and Table 1) yield

485   minimum CRE ages of 17.5 ± 3.7 ka and 20.0 ± 2.9 ka, respectively. Northeast of the channel

486   the General Carrera shoreline area exhibits the moraine overlaying fan-delta sediment. At this

487   site the moraine has removed the upper part of the terrace. However, the internal bedding of

488   the terrace documents delta growth towards the General Carrera Lake. We infer that the Lago

489   Bertrand outlet was flowing eastward, in opposite direction as compared to the situation at

490   Present. Strandlines notch deeply the moraine ridge documenting subsequent flooding.

491   Finally, drainage to the west has induced ~100 m incision of the channel spillway to Lago

492   Bertrand.

493   The Lago Negro (Fig. 13) with water level at ~ 235 m elevation shows no outlet at Present.

494   To the west, a bare rock dome of metamorphic rock prevents connection with the Lago

495   Bertrand. This metamorphic basement exhibits large –i.e. hundred of meters long– drumlins

496   documenting ice flow to the east. East of Lago Negro, a ~ 30 to 100 m high moraine ridge

497   obstructs the pathway towards the General Carrera Lake. A [10]Be mean age of 11.2 ± 1.3 ka

498   for three samples has been documented for this moraine (Glasser et al., 2012) suggesting that

499   the ice lobe re-advance at this site occurred during the YD. This moraine unconformably

500   overlies a thick fan-delta accumulation (Fig. 13 B and D) displaying foreset layers dipping

501   towards the General Carrera Lake –i.e. to the NE–. Because the moraine has abraded most of

502   the fan-delta topset layers, no precise elevation of the upper part of the corresponding terrace

503   is known. However, a minimum elevation of ~300 m is documented that allows us to assign

504 the fan-delta to the T1 terrace episode. A thick T1 terrace accumulation located along the
505 southern rim of the Lago Negro corroborates this assumption (sampling site 39, Fig. 13 A).
506 This terrace showing a well-preserved topset layers at ~364 m (highest elevation) exhibits
507 several dropstones. One of them (Fig. 5 C) yields a minimum CRE age of 14.4 ± 3.0 ka
508 (sample 39, Table 1). Northwest of the Lago Negro moraine (Fig. 13 A and C) pervasive
509 strandlines exist between 300 and 400 m elevation. The lower strandlines notch the moraine
510 that documents a fluctuating lake level and a subsequent flooding of the moraine. Northwest
511 of the main moraine outcrop (Fig. 13 A and B) a morphological depression exists. At this site,
512 the moraine has been removed by erosion suggesting that a higher transgressive episode of
513 the lake has favored water routing from the Lago Negro to the General Carrera Lake. This
514 reinforces the conceptual model proposed by Hein et al. (2010), Bell (2008) and Turner
515 (2005) who have proposed that the PC Lake out flowed toward the GCBA Lake through the
516 Rio Baker valley as caused by ice-damming preventing any discharge towards the Pacific.
517 The geomorphological analyses of the Lago Negro and Lago Bertrand outlet areas and their
518 evolution (Fig. 13) allow disentangling their development through time. First, a thick fan-
519 delta accumulated, which elevation allows ascribing the sediment accumulation to the T1
520 terrace event. The fan delta forset layers (Fig. 13 D) document that stream-discharge was
521 flowing eastward from the Lago Negro and Lago Bertrand towards the General Carrera Lake.
522 Subsequently a prominent ridge moraine developed unconformably overlying the fan-delta
523 accumulations and the basement rock. The ice was flowing to the east. Because strandlines
524 notch the moraines (Fig. 12 B and C, 13 C) we infer that a major transgression event occurred
525 afterward, flooding the moraine ridge.
526
527 4.7. Rio Bayo/Rio Tranquilo area
528
529   The short depression along the Rio Tranquilo (flowing to the GCBA Lake) connecting to
530 the Rio Bayo (flowing to the Pacific Ocean) marks the Present northern boundary of the NPI.
531 The divide between the two rivers is at 371 m elevation. The Rio Tranquilo exhibits the
532 typical morphology of a deep narrow glacial valley. The terminal moraine of a major glacier
533 flowing northward from the NPI is damming the valley floor of the Rio Bayo. Glasser et al.
534 (2005) have proposed that this terminal moraine dated back to the Little Ice Age.
535 Subsequently, Glasser et al. (2006) have documented that ice mass remained in the Rio Bayo
536 outlet glacier until 9.7 ± 0.7 ka. Whatever is the age of the major ice recession along the Rio

537 Bayo/Rio Tranquilo depression, we do note that no erosion associated to the subsequent water
538 drainage exists at the divide between the GCBA Lake and the Pacific. It suggests that the
539 valley has never been a significant spillway for the GCBA Lake.
540

5. Discussion

542

5.1. Ice retreat, water routing, and climate inferences

544

545   The Buenos Aires Lake area (Argentina) has recorded two morpho-climatic stages. The
546 first stage, which extends from the LGM (19-27 ka) to the ACR (12.9-14.5 ka), exhibits six
547 ice lobe re-advances or still-stands recorded by the Menucos and Fenix I to V moraine ridges.
548 The ice lobe had an oscillatory development, the cold episodes being separated by warmer
549 periods of retreating ice front. No evidence exists for major retreats, the ice lobe remaining
550 located along the Andean foreland. We infer modest climate fluctuations at the millennium
551 time scale till the ACR. Water routing was from a pro-glacial lake toward the Atlantic Ocean.
552 During the second stage the Buenos Aires Lake became free of ice and evolved as a major pro
553 glacial lake for the remaining General Carrera ice lobe. The water level of the pro-glacial lake
554 was controlled by the elevation of the Perito Moreno outlet (392 m at Present). Because (1)
555 the braided pattern areas (Fig. 8) show no evidence for subsequent lake flooding higher than
556 415 ± 5 m, and (2) the Rio Deseado spillway exhibits a very low water flow associated with
557 no active erosion, we assume a significant rainfall deficit in this rain shadow area at the origin
558 of the ice retreat following the ACR. A drainage re-arrangement occurred during the
559 transition from stage 1 to stage 2 through the capture of the Rio Fenix Grande by the Rio
560 Fenix Chico. No Significant water drainage toward the Atlantic Ocean existed at that time.
561 Since then the GCBA Lake became an endorheic basin.
562   Five different episodes (T0 to T4, Table 2) of terrace development have recorded the
563 evolution of the shoreline area of the General Carrera Lake. Since, the terrace T1 is older than
564 the moraines described by Douglass et al. (2005) at Fachinal (revised ages at 10.9 ± 1.3 ka),
565 the more elevated terraces —i.e. T2 to T4 terraces— should be older. The oldest minimum
566 CRE age obtain for dropstones on terraces (18.8 ± 3.9 ka, sample 71, Terrace T4, Table 1)
567 constrains the maximum age for terraces accumulation. Also the accumulation of terraces T2
568 to T4, which evolved in an ice-walled lake environment along the main ice lobe of the
569 General Carrera glacier, has likely to occur during the ACR from 12.9 to 14.5 ka. We

570 therefore infer that the accumulation of the terraces T1 to T4 occurred between 12.9-14.5 and

571 10.9 ± 1.3 ka. The T0 terrace likely began accumulating after the younger Inner moraine at

572 Facinal —age at 7.9 ± 1.1 ka— that is in agreement with the age (younger than 6.7 ka)

573 proposed by Bell (2008).

574   The accumulation of the T1 terrace, which extends all along both sides of the General

575 Carrera Lake (Fig. 14), documents a period of relatively stable lake level associated with

576 massive ice retreat. The western outlet area of the General Carrera Lake indicates that the Rio

577 Baker was flowing eastward and draining the CP Lake watershed during that period. Turner et

578 al. (2005) have first proposed such a drainage scenario. Subsequently, Hein et al. (2010)

579 assumed the drainage system being active for the time window 15-16.5 ka. We regard the

580 youngest limit to be too old by about ~ 0.5 ka as a minimum. This drainage organization

581 indeed suggests that ice damming along the Rio Baker was prohibiting any discharge to the

582 Pacific. Because no significant drainage toward the Atlantic also existed during the time

583 period from 12.9-14.5 to 10.9 ± 1.3 ka, we infer that the Terrace T1 accumulated in an

584 endorheic environment controlled by a severe rainfall deficit.

585   At the Lago Negro and Lago Bertrand spillways (GCBA Lake western outlet), moraine

586 ridges overly the T1 terrace (Fig. 12 and 13). At both sites, the moraines were subsequently

587 flooded. Two major morpho-climatic events punctuated the evolution of the GCBA Lake area

588 after the terrace T1 accumulation. It includes a glacial advance during a neoglacial activity

589 followed by a major flooding event. The post terrace T1 glacial advance was first documented

590 and dated at Fachinal where two short episodes of glacier advance occurred at 10.9 ± 1.3 and

591 7.9 ± 1.1 ka. These two cold events may correlate the YD and the 8.2 Cold Event. Whatever

592 they are, they have likely recorded an increase in precipitation and/or a decrease in

593 temperature resulting from a northward migration of the Westerlies.

594   Subsequently, a major flooding of the two Holocene moraines re-advances occurred as

595 documented at the GCBA Lake outlet area. Also, at the Rio de Las Dunas area (Fig. 9 and 10)

596 a pervasive strandline imprint documents this major transgression phase. Topsets and cliffs of

597 the T1 to T4 terrace fan-deltas exhibit regularly spaced notches and strandlines (tempestites)

598 extending from 527 m to the lake level (201 m) at Present. The regularly nested shoreline

599 pattern punctuate by storms suggests a steady smooth lowering of the lake from 527 m to 201

600 m. As exemplified at point X (Fig. 9), cold/wet events such as the Little Ice Age occurred

601 during lake lowering phases. The dry climate and the incision of the Bertrand Lake outlet are

602 the main processes at the origin of the GCBA Lake regression that occurred after the last

603 major re-advance of glaciers at 7.9 ± 1.1 ka. This regression is documented by drop-stones

604 sampled at the 53 and 73 sites (Fig 12 C and Fig. 9, respectively, and Table 1). Indeed, (1)

605 sample 53 yields a minimum CRE age at 8.6 ± 2.0 ka, a mid point age close to the 8.2-ka

606 Cold Event as is the second cold event identified at Fachinal —i.e. the Inner moraine

607 described by Douglass et al., (2005), mid point age at 7.9 ka—, (2) sample 73 that yields a

608 minimum CRE age at 9.9 ± 2.5 ka has been collected overlying a tempestite ridge at 521 m

609 elevation. Therefore, the emplacement of the dropstone (sample 73) has to occur during the

610 major flooding event following the second cold event at 7.9 ± 1.1 ka. Although ages of

611 samples 53 and 73 are imprecise, they provide evidences for climate events —i.e. the 8.2-ka

612 Cold Event and the subsequent flooding event— occurring during/or after the 8.2-ka Cold

613 Event.

614   The General Carrera Lake has recorded five morpho-climatic episodes. During the first

615 episode, T2 to T4 terraces accumulated in ice-walled lake environment, as a major ice tongue

616 existed along the General Carrera Lake. During the second episode, the disintegration of the

617 ice tongue allowed a general distribution of the T1 terrace along the General Carrera Lake.

618 Subsequently, two major ice advance occurred at ~10.9 ± 1.3 ka and ~7.9 ± 1.1 ka during the

619 third episode. The fourth episode matches a general flooding that has reached the elevation of

620 the highest T4 terrace. Because no evidence exists for the Perito Moreno eastern outlet being

621 active in association with ice damming preventing drainage to the Pacific, we infer that the

622 flooding event resulted from a rainfall enhancement after 7.9 ± 1.1 ka. The fifth episode

623 began as the western outlet opened and allowed drainage to the Pacific with no major

624 disruption till the Present. We consider that all five episodes controlling the evolution of the

625 General Carrera Lake post-date the first stage identified at the Buenos Aires Lake. Although

626 the age and extent of the ACR is latitudinal controlled and controversial, it is accepted as a

627 valuable age control for the colonization of recently deglaciated terrains by forests of

628 *Nothofagus* ca. 12.3 ago (Moreno et al., 2009) at Torres del Paine area (~51°S).

629

630 ## 5.2. Glacial rebound

631

632   In a low viscosity regime of 1 x 10^{18} Pa s for the asthenosphere associated with an elastic

633 lithosphere thickness of 35 km, Ivins and James (2004, 1999) have predicted rates of crustal

634 vertical motion similar to those presently occurring in Fennoscandia, and eastern Canada

635 (Lambeck et al., 1998; Wu, 1997; Mitrovica and Forte, 1997; Mitrovica and Peltier, 1992).

636 Estimating ice volume loss for the past 4-5 ka, they calculated crustal uplift rates of 5 to 12

mm.yr^{-1} for the NPI and SPI. Based on Global Positioning System (GPS) measurements performed between 2003 and 2006, Dietrich et al. (2010) have documented a vertical crustal uplift rate of 39 mm.yr^{-1} for the SPI. This uplift rate is an order of magnitude higher than previously anticipated. They infer a response to an accelerated glacier wasting since the termination of the Little Ice Age (LIA) consistent with an effective regional mantle viscosity of ~ 4.0-8.0 x 10^{18} Pa s. This low viscosity would originate from the asthenospheric mantle flow associated with the Patagonia slab window at depth. In addition, Dietrich et al. (2010) have anticipated the ability of even lower viscosity than those reported from young and dynamic volcanic regions due to the massive influx of volatiles through the slab window (Gorring and Kay, 2001). Dietrich et al. (2010) have documented that the large GPS uplift rates are generated by an integral response to glacier losses since the termination of the LIA in the late 19th Century.

Our data together with those of Douglass et al. (2005) allow reconstructing the morpho-tectonic situation by the end of the major transgression occurring after the ice re-advance at 7.9 ± 1.1 ka (Fig. 15). (1) East of the GCBA Lake, the elevation of the divide at Perito Moreno (392 m at Present) is not accurately documented. From simple models, Ivins and James (2004; 1999) have predicted 1 mm.yr^{-1} of vertical motion at the divide. Depending on the accepted glacier fluctuations, they have inferred both uplift and subsidence occurring during the Late Holocene and Present based on a likely elevation of ~ 392 ± 6 m at 7.9 ± 1.1 ka. From GPS measurements, Dietrich et al. (2010) have extrapolated an uplift rate resulting from the SPI mass loss of 0.4-0.8 mm.yr^{-1} for the area located between Chile Chico and Perito Moreno (Fig. 7). No uplift value resulting from the NPI ice loss is proposed. Finally, we consider the Present elevation (392 m) of the divide as a conservative value for our rebound calculation along the GCBA Lake (see below). (2) South of the Rio de Las Dunas fan-delta (Fig. 9 and 10), we have documented that the General Carrera Lake was at 326 m above its present elevation (201 m). Whether no tectonic deformation is considered for the past 7.9 ± 1.1 ka, a lake level higher than the outlet at Perito Moreno must be considered. Therefore, we must consider an uplift correction that is the difference between the most elevated shoreline at 7.9 ± 1.1 ka (527 m) and the elevation at the Perito Moreno outlet (392 m or less). Based on the Perito Moreno outlet elevation at 7.9 ± 1.1 ka ago, a minimum uplift of 135 m for the Rio de Las Dunas area has thus to be considered. (3) West of the GCBA Lake, at the Lago Bertrand outlet (Fig. 12), two main bodies of evidences have been considered. First, flooding of the 10.9 ± 1.3 to 7.9 ± 1.1 ka moraines occurred during a major transgression episode that reached 527 m at the Rio de Las Dunas, the lake elevation at both sites —i.e. the Rio de Las

671 Dunas and the Lago Bertrand outlet— being controlled by ice damming along the Rio Baker.

672 Second, the incision at the Lago Bertrand outlet has completely removed the moraine ridge

673 accumulated at 10.9 ± 1.3 to 7.9 ± 1.1 ka. Because the unconformity of the underlying T1

674 terrace with the basement rock is not clearly identified, no confident incision measurement is

675 possible at this site. Considering that the GCBA Lake is the local base level for its tributaries,

676 an incision at the Lago Bertrand outlet from incision measurement at tributaries was

677 calculated. The Rio Müller (Fig. 11) and Rio El Salto (Fig. 3 D), two of the lake tributaries,

678 have recorded incisions of 94 and 102 m, respectively. We therefore infer that a down cutting

679 of ~ 98 m (average of incision along tributaries) has occurred at the GCBA Lake outlet

680 documenting an incision rate of 10.9 to 14.4 mm.yr^{-1} for the past 7.9 ± 1.1 ka.

681 The ~ 326 m amplitude of lake level variation (Fig. 15) should be split into an incision

682 signal of ~ 98 m and a remaining rebound signal of 228 m (maximum value). A rebound

683 signal ranging from 228 to 135 m highlighted in an area located at Rio de Las Dunas yields to

684 an uplift rate between 15 and 33.5 mm.yr^{-1} for the past 7.9 ±1.1 ka. Assuming a permanent

685 rainfall deficit in this rain shadow area, the largest uplift rate is the most likely. If accepted,

686 this assumption implies that the average uplift rate at the Rio de Las Dunas area calculated

687 over the past 7.9 ± 1.1 ka is in the same order than that derived from the GPS measurements

688 (39 mm.yr^{-1}) performed between 2003 and 2006 along a SPI transect (Dietrich et al., 2010).

689 Considering the slab window-induced low viscosity at depth and the elastic lithosphere

690 thickness as local invariants, we infer that the high uplift rates calculated over the past 7.9

691 ± 1.1 ka originated mainly from ice loss as it was proposed for the time period following the

692 termination of the LIA. We suggest that (1) massive ice loss occurred not only during the last

693 century but dated back to several ka in the past, and (2) the ice re-advances at 7.9 ± 1.1 ka is

694 likely more significant than anticipated.

695

696 6. Conclusions

697

698 • Relative chronology of morpho-climatic records together with 18 cosmogenic [10]Be

699 ages and available data allow us constraining the timing of the Patagonian ice-sheet

700 fluctuations since the LGM.

701 • The estimated thickness of ice along the GCBA lobe at the longitude of Chile Chico

702 (Argentina-Chile border) is ~1.5 to 1.7 km during the LGM. The estimated ELA at

that time is ~1100 m (no rebound correction), an elevation similar to that proposed for the Chilean Lakes region during the LGM.

- The Buenos Aires Lake area (Argentina) has recorded two morpho-climatic stages. The first one extends from the LGM (19-27 ka) to the ACR (12.9-14.5 ka). The ice lobe front has been oscillating at the millennial scale remaining located along the Andean foreland. During the second stage the Buenos Aires Lake became free of ice. A significant rainfall deficit in this rain shadow area was coeval with the ice retreat following the ACR, the GCBA Lake becoming an endorheic basin.

- The General Carrera Lake evolved through five morpho-climatic episodes, all likely younger than 12.9-14.5 ka. During the first and the second episode the lake evolved as an endorheic basin from 10.9 ± 1.3 to 12.9 ka. Two cold events associated with glacier re-advance occurred at 7.9 ± 1.1 and 10.9 ± 1.3 ka during the third episode. These cold events may relate to the 8.2-ka Cold Event and the YD, respectively. A major flooding younger than 7.9 ± 1.1 ka resulted from a rainfall enhancement occurring during the fourth episode. The fifth episode began as the western outlet of the GCBA Lake opened allowing drainage to the Pacific with no major disruption till the Present

- We highlight a rebound signal ranging from 135 m to 228 m in an area located at Rio de Las Dunas (General Carrera Lake). The uplift rate (glacial rebound) ranges between 15 and 33.5 mm.yr^{-1} for the past 7.9 ± 1.1 ka.

- The average uplift rate of the Rio de Las Dunas area calculated over the past 7.9 ± 1.1 ka is in the same order than the GPS measurements (39 mm.yr^{-1}) performed between 2003 and 2006 along a SPI transect (Dietrick et al., 2010). We infer that the high uplift rates calculated over the past 7.9 ± 1.1 ka mainly resulted from ice loss.

- We suggest that (1) massive ice loss occurred not only during the last century but dated back to several ka, and (2) the ice re-advance at 7.9 ± 1.1 ka is more significant than previously thought.

- A down cutting of ~ 98 m has occurred at the western GCBA Lake outlet documenting an elevated incision rate of 10.9 to 14.4 mm.yr^{-1} during the past 6.8-9 ka.

740

References

742

743 Ackert, Jr.R.P.; Singer, B.S.; Guillou, H.; Kaplan, M.R.; and Kurz, M.D. 2003. Long-term
744   cosmogenic ^{3}He production rates from ^{40}Ar/^{39}Ar and K-Ar dated Patagonian lava flows at
745   47°S. Earth and Planetary Science Letters 210, 119-136.

746

747 Alley, R.B. 2000. The Younger Dryas cold interval as viewed from central Greenland.
748   Quaternary Science Reviews 19, 213-226.

749

750 Alley, R.B.; Mayewski, P.A.; Sowers, T.; Stuiver, M.; Taylor, K.C.; and Clark, P.U. 1997.
751   Holocene climatic instability: a prominent, widespread event 8200 yr ago. Geology 25,
752   483-486. doi: 10.1130/0091-7613(1997)025<0483:HCIAPW>2.3.CO;2.

753

754 Aniya, M.; Sato, H.; Naruse, R.; Skvarca, P.; Casassa, G. 1996. The use of satellite and
755   airborne imagery to inventory outlet glaciers of the Southern Patagonia Icefield, South
756   America. Photogrammetric Engineering & Remote Sensing 62, 1361-1369.

757

758 Aniya, M. 1988. Glacier inventory for the Northern Patagonia Icefield, Chile, and variations
759   1944/45 to 1985/86. Arctic, Antarctic and Alpine Research 20, 179-187.

760

761 Bakke J.; Nesje, A. 2011. The equilibrium line altitude (ELA): Encyclopedia of snow, ice and
762   glaciers. Springer, 268-277.

763

764 Bell, C.M. 2008. Punctuated drainage of an ice-dammed Quaternary lake in southern South
765   America. Geografiska Annaler 90, 1-17.

766

767 Behrmann, J.H.; Lewis, S.D.; and ODP Leg 141 Scientific Party 1992. Geology and tectonics
768   of the Chile triple junction. Eos (Transactions, American Geophysical Union) 73, 404-405,
769   410.

770

771   Blard, P-H.; Braucher, R.; Lavé, J.; Bourlès, D.L. 2013. Cosmogenic [10]Be Production Rate

772   Calibrated Against [3]He in the High Tropical Andes (3800-4900 m, 20-22°S). Earth and

773   Planetary Science Letters 382, 140-149.

774

775   Boex, J.; Fogwill, C.; Harrison, S.; Glasser, N.F.; Hein, A.; Schnabel, C.; Xu, S. 2013. Rapid

776   thinning of the late Pleistocene Patagonian Ice Sheet followed migration of the Southern

777   Westerlies. Nature Scientific Reports 3, 2118, DOI:10.1038/srep02118.

778

779   Bourgois, J.; Michaud, F. 2002. Comparison between the Chile and Mexico triple junction

780   areas substantiates slab window development beneath northwestern Mexico during the past

781   12-10 Myr. Earth and Planetary Science Letters 201, 35-44.

782

783   Bourgois, J.; Guivel, C.; Lagabrielle, Y.; Calmus, T.; Boulègue, J.; and Daux, V. 2000.

784   Glacial-interglacial trench supply variation, spreading-ridge subduction, and feedback

785   controls on the Andean margin development at the Chile triple junction area (45-48°S).

786   Journal of Geophysical Research 105, 8355-8386.

787

788   Bourlès, D. L. 1988. Etude de la géochimie de l'isotope cosmogénique [10]Be et de son isotope

789   stable en milieu océanique. Application à la datation de sediments marins. PhD, Paris Sud

790   Centre d'Orsay University, Orsay, France.

791

792   Braucher, R.; Merchel, S.; Borgomano, J.; Bourlès, D.L. 2011. Production of cosmogenic

793   radionuclides at great depth: a multi element approach. Earth and Planetary Science Letters

794   309(1-2), 1-9.

795

796   Breitsprecher, K.; and Thorkelson, D.J. 2009. Neogene kinematic history of Nazca-Antarctic-

797   Phoenix slab windows beneath Patagonia and Antartic Peninsula. Tectonophysics 464, 10-

798   20.

799

800   Brown, E. T.; Brook, E.J.; Raisbeck, G.M.; Yiou, F.; and Kurz, M.D. 1992. Effective

801   attenuation lengths of cosmic producing 10Be and 26Al in quartz, implications for

802   exposure age dating. Geophysical Research Letters 19, 369– 372.

803

804   Brown, E.T.; Edmond, J.M.; Raisbeck, G.M.; Yiou, F.; Kurz, M.D.; Brook, E.J. 1991.

805   Examination of surface exposure ages of Antarctic moraines using in situ produced [10]Be

806   and [26]Al. Geochimica et Cosmochimica Acta 55, 2269–2283.

807

808   Caldenius, C.G. 1932. Las glaciaciones Cuaternarias en la Patagonia and Tierra de Fuego.

809   Geografiska Annaler 14, 1-164.

810

811   Cande, S.C.; and Leslie R.B. 1986. Late Cenozoic tectonics of the southern Chile trench.

812   Journal of Geophysical Research 92, 495-520.

813

814   Casassa, G. 1987. Ice thickness deduced from gravity anomalies on Soler glacier, Neff glacier

815   and the northern Patagonia Icefield. Bulletin of Glacier Research 4, 43-57.

816

817   Chmeleff, J.; von Blanckenburg, F.; Kossert, K.; and Jakob, J. 2010. Determination of the

818   [10]Be half-life by multicollector ICP-MS and liquid scintillation counting. Nuclear

819   Instruments and Methods in Physics Research B 268, 192–199.

820

821   Clapperton, C.M. 1997. Fluctuations of local glaciers 30-8 ka B.P.: overview. Quaternary

822   International 38/39, 3-6.

823

824   DeLong, S.E.; Fox, P.J.; MacDowell, F.W. 1978. Subduction of the Kula Ridge at the

825   Aleutian Trench: Geological Society of America Bulletin 89, 83-95.

826

827   Dickinson, W.R.; Snyder, W.S. 1979. Geometry of subducted slabs related to San Andreas

828   transform. Journal of Geology 87, 609-627.

829

830   Dietrich, R.; Ivins, E.R.; Casassa, G.; Lange, H.; Wendt, J.; Fritsche, M. 2010. Rapid crustal

831   uplift in Patagonia due to enhanced ice loss. Earth and Planetary Science Letters 289, 22-

832   29.

833

834   Douglass, D.C.; Singer, B.S.; Kaplan, M.R.; Mickelson, D.M.; Caffee, M.W. 2006.

835   Cosmogenic nuclide surface exposure dating of boulders on last-glacial and late-glacial

836   moraines, lago Buenos Aires, Argentina: interpretative strategies and paleoclimate

837   implications. Quaternary Geochronology 1, 43-58.

838

839 Douglass, D.C.; Singer, B.S.; Kaplan, M.R.; Ackert, R.P.; Mickelson, D.M.; Caffee, M.W.
840   2005. Evidence of early Holocene glacial advances in southern South America from
841   cosmogenic surface-exposure dating. Geology 33, 237-240.

842

843 Fleming, K.; Johnston, P.; Zwartz, D.; Yokoyama, Y.; Lambeck, K.; Chappell, J. 1998.
844   Refining the eustatic sea-level curve since the Last Glacial Maximum using far- and
845   intermediate-field sites. Earth and Planetary Science Letters 163, 327-342.

846

847 Garreaud, R.; Lopez, P.; Minvielle, M.; and Rojas, M. 2013. Large-scale control on the
848   Patagonia climate. Journal of Climate, American Meteorological Society 26, 215-230,
849   DOI: 10.1175/JCLI-D-12-00001.1.

850

851 Glasser, N.F., Harrison, S.; Schnabel, C.; Fabel, D.; Jansson K.N. 2012. Younger Dryas and
852   early Holocene age glacier advances in Patagonia. Quaternary Science Reviews 58, 7-17.

853

854 Glasser, N.F.; Harrison, S.; Ivy-Ochs, S.; Duller, G. A. T.; Kubik, P. W. 2006. Evidence from
855   the Rio Bayo valley on the extent of the North Patagonian Icefield during the Late
856   Pleistocene-Holocene transition. Quaternary Research 65, 70-77.

857

858 Glasser, N.F.; Jansson, K.N.; Harrison, S.; Rivera, A. 2005. Geomorphological evidence for
859   variations of the North Patagonian Icefield during the Holocene. Geomorphology 71, 263-
860   277.

861

862 Gorring, M.; Singer, B.; Gowers, J.; and Kay, S. 2003. Plio-Pleistocene basalts from the
863   Meseta del Lago Buenos Aires, Argentina: evidence for asthenosphere-lithosphere
864   interactions during slab window magmatism. Chemical Geology 193, 215-235.

865

866 Gorring, M.; and Kay, S. 2001. Mantle processes and sources of Neogene slab window
867   magmas from southern Patagonia. Argentina. Journal of Petrology 42, 1067–1094.
868   doi:10.1093/petrology/42.6.1067.

869

870 Gorring, M.L.; Kay, S.M.; Zeitler, P.K.; Ramos, V.A.; Rubiolo, D.; Fernandez, M.I.; and
871   Panza, J.L. 1997. Neogene Patagonian plateau lavas: continental magmas associated with
872   ridge collision at the Chile triple junction. Tectonics 16, 1-17.
873

874 Guivel, C.; Morata, D.; Pelleter, E.; Espinoza, F.; Maury, R.; Lagabrielle, Y.; Polvé, M.;
875   Bellon, H.; Cotton, J.; Benoit, M.; Suarez, M.; de la Cruz, R. 2006. Miocene to Late
876   Quaternary Patagonian basalts (46-47° S): geochronometric and geochemical evidence for
877   slab tearing due to active spreading ridge subduction. Journal of Volcanology and
878   Geothermal Research 149, 346-370.
879

880 Hein, A.S.; Hulton, N.R.J.; Dunai, T.J.; Sugden, D.E.; Kaplan, M.R.; Xu, S. 2010. The
881   chronology of the Last Glacial Maximum and deglacial events in central Argentine
882   Patagonia. Quaternary Science Reviews 29, 1212-1227.
883   doi:10.1016/j.quascirev.2010.01.020
884

885 Hein, A.S.; Hulton, N.R.J.; Dunai, T.J.; Schnabel, C.; Kaplan, M.R.; Naylor, M.; Xu, S. 2009.
886   Middle Pleistocene glaciation in Patagonia dated by cosmogenic-nuclide measurements on
887   outwash gravels. Earth and Planetary Science Letters 286, 184-197,
888   Doi:10.1016/j.epsl.2009.06.026
889

890 Hoffman, J.A.J. 1975. Atlas Climatico de America del Sur. WMO, Unesco, Geneva.
891

892 Hulton, N.R.J.; Purves, R.S.; McCulloch, R.D.; Sugden, D. E.; Bentley, M.J. 2002. The Last
893   Glacial Maximum and deglaciation in southern South America. Quaternary Science
894   Reviews 21, 233-241.
895

896 Hulton, N.R.J.; and Sugden, D.E. 1997. Dynamics of mountain ice caps during glacial cycles:
897   the case of Patagonia. Annals of Glaciology 24, 81-89.
898

899 Hulton, N.D.; Sugden, D.; Payne, A.; and Clapperton, C. 1994. Glacier modeling and climate
900   of Patagonia during the last glacial maximum. Quaternary Research 42, 1-19.
901

902 Ivins, E.R.; and James, T.S. 2004. Bedrock response to Llanquihue Holocene and present-day
903   glaciation in southernmost South America. Geophysical Research Letters 31, L24613,
904   doi:10.1029/2004GL021500.
905

906 Ivins, E.R.; and James, T.S. 1999. Simple models for late Holocene and Present-day
907   Patagonian glacier fluctuations and predictions of a geodetically detectable isostatic
908   response. Geophysical Journal International 138, 601-624.
909

910 Jomelli, V.; Favier, V.; Vuille, M.; Braucher, R.; Martin, L.; Blard, H.; Colose, C.; Brunstein,
911   D.; He, F.; Khodri, M.; Bourles, D.; Leanni, L.; Rinterknecht, V.; Grancher, D.; Francou,
912   B.; Ceballos, J.L.; Fonseca, H.; Liu, Z.; and Otto-Bliesner, B.L. 2014. A major advance of
913   tropical Andean glaciers during the Antarctic cold reversal. Letter to Nature,
914   doi:10.1038/nature13546.
915

916 Kaplan, M.R.; Strelin, J.A.; Schaefer, J.M.; Denton, G.H.; Finkel, R.C.; Schwartz, R.;
917   Putnam, A.E.; Vandergoes, M.J.; Goehring, B.M.; Travis, S.G. 2011. In-situ cosmogenic
918   [10]Be production rate at Lago Argentino, Patagonia: Implications for late-glacial climate
919   chronology. Earth and Planetary Science Letters 309, 21–32.

920

921 Kaplan, M.R.; Ackert, R.P.; Singer, B.S.; Douglass, D.C.; and Kurz, M.D. 2004. Cosmogenic
922   nuclide chronology of millennial-scale glacial advances during O-isotope stage 2 in
923   Patagonia. Geological Society of America Bulletin 116, 308-321, doi: 10.1130/B25178.1.
924

925 Kelly, M.A.; Lowell, T.V.; Applegate, P.J.; Phillips, F.M.; Schaefer, J.M.; Smith, C.A.; Kim,
926   H.; Leonard, K.C.; and Hudson A.M. 2014. A locally calibrated, late glacial [10]Be
927   production rate from a low-latitude, high-altitude site in the Peruvian Andes. Quaternary
928   Geochronology, http://dx.doi.org/10.1016/j.quageo.2013.10.007
929

930 Klemann, V.; Ivins, E.R.; Martinec, Z.; and Wolf, D. 2007. Models of active glacial isostasy
931   roofing warm subduction: case of the South Patagonia Icefield. Journal of Geophysical
932   Research 112, B09405, doi:10.1029/2006JB004818.
933

934 Korschinek, G.; Bergmaier, A.; Faestermann, T.; Gerstmann, U.C.; Knie, K.; Rugel, G.;
935   Wallner, A.; Dillmann, I.; Dollinger, G.; Lierse von Gostomski, Ch.; Kossert, K.; Maitia,
936   M.; Poutivtsev, M.; and Remmert, A. 2010. A new value for the half-life of 10Be by
937   Heavy-Ion Elastic Recoil Detection and liquid scintillation counting. Nuclear Instruments
938   and Methods in Physics Research B. 268, 187–191.
939

940 Lal, D. 1991a. The present scope of the field of terrestrial cosmogenic nuclides. Science 6,
941   744-751.
942

943 Lal, D. 1991b. Cosmic ray labeling of erosion surfaces: In situ nuclide production rates and
944   erosion models. Earth and Planetary Science Letters 104, 424–439,
945

946 Lambeck, K., Smither, C., and Johnston, P., 1998. Sea-level change, glacial rebound and
947   mantle viscosity for northern Europe. Geophysical Journal International 134, 102-144.
948

949 Leslie, R.B. 1986. Cenozoic tectonics of southern Chile triple junction migration, ridge
950   subduction, and forearc evolution. PhD thesis, 276 pp., Columbia University, New York.
951

952 Lowell, T.V.; Heusser, C.J.; Andersen, B.G.; Moreno, P.I.; Hauser, A.; Heusser, L.E.;
953   Schlüchter, C.; Marchant, D.R.; and Denton, G.H. 1995. Interhemispheric correlation of
954   Late Pleistocene glacial events. Science 269, 1541-1549.
955

956 Marden, C.J.; and Clapperton, C.M. 1995. Fluctuations of the South Patagonia Icefields
957   during the last glaciation and the Holocene. Journal of Quaternary Science 10, 197-210.
958

959 Markgraf, V.; Dodson, J.R.; Kershaw, A.P.; McGlone, S.; and Nicholls, N. 1992. Evolution
960   of Late Pleistocene and Holocene climates in the circum-South Pacific land areas. Climate
961   Dynamics 6, 193-211.
962

963 Mercer, J.H. 1982. Holocene glacier variations in Southern South America. Striae 18, 35-40.
964

965 Merchel, S.; and Herpers, U. 1999. An update on radiochemical separation techniques for the
966   determination of long-lived radionuclides via Accelerator Mass Spectrometry.
967   Radiochimica Acta 84, 215–219.

968

969 Miller, A. 1976. The climate of Chile, in World Survey of Climatology, vol. 12. Climates of
970   Central Chile and South America, edited by W. Schwerdtferger, 113-145, Elsevier,
971   Amsterdam-Oxford-New York.

972

973 Mitrovica, J.X.; and Forte, A. 1997. Radial profile of mantle viscosity: results from the joint
974   inversion of convection and post-glacial rebound observables. Journal of Geophysical
975   Research 102, 2751-2769.

976

977 Mitrovica, J.X.; and Peltier, W.R. 1992. Constraints on mantle viscosity from relative sea
978   level variations in Hudson bay. Geophysical Research Letters 19, 1185-1188.

979

980 Moreno, P.L.; Kaplan, M.R.; François, J.P.; Villa-Martinez, R.; Moy, C.M.; Stern, C.R.;
981   Kubik, P.W. 2009. Renewed glacial activity during the Antarctic Cold Reversal and
982   persistence of cold conditions until 11.5 ka in southwestern Patagonia. Geology 37, 375-
983   378. doi: 10.1130/G25399A.

984

985 Murdie, R.E.; Pugh, D.T.; Styles, P. 1999. A lightweight, portable, digital probe for
986   measuring the thermal gradient in shallow water sediments, with examples from Patagonia.
987   Geo-Marine Letters 18, 315-320.

988

989 Orihashi, Y.; Anma, R.; Motoki, A.; Haller M.J.; Hirata, D.; Iwano, H.; Sumino, H.; Ramos,
990   A. 2013. Evolution history of the crust underlying Cerro Pampa, Argentine Patagonia:
991   constraint from LA-ICPMS U-Pb ages for exotic zircons in the Mid-Miocene adakite.
992   Geochemical Journal 47, 235-247.

993

994 Peck, V.L.; Hall, I.R.; Zahn, R.; Grousset, F.; Hemming, S.R.; Scourse, J.D. 2007. The
995   relationship of Heinrich events and their European precursors over the past 60 ka BP: a
996   multi-proxy ice-rafted debris provenance study in the northeast Atlantic. Quaternary
997   Science Reviews 26, 862-875. doi:10.1016/j.quascirev.2006.12.002.

998

999 Porter, S.C. 1981. Pleistocene glaciation in the southern Lake District of Chile. Quaternary
1000   Research 16, 263-292.

1001

1002 Raisbeck, G. M.; Yiou, F.; Bourles, D. L.; Brown, E.T.; Deboffle, D.; Jouhanneau, P.;
1003   Lestringuez, J.; and Zhou, Z.Q. 1994. The AMS facility at Gif-sur-Yvette: Progress,
1004   perturbations and projects. Nuclear Instruments and Methods in Physics Research B92, 43-
1005   46.

1006

1007 Raisbeck, G. M.; Yiou, F.; Bourlès, D.L.; Lestringuez, J.; and Deboffle, D. 1987.
1008   Measurements of ^{10}Be and ^{26}Al with a Tandetron AMS facility. Nuclear Instruments and
1009   Methods in Physics Research B29, 22-26.

1010

1011 Rivera, A.; Benham, T.; Casassa, G.; Bamber, J.; Dowdeswell, J.A. 2007. Ice elevation and
1012   areal changes of glaciers from the northern Patagonia Icefield, Chile. Global and
1013   Planetary Change 59, 126-137.

1014

1015 Russo, R.M.; VanDecar, J.C.; Comte, D.; Mocanu, V.I.; Gallego, A.; and Murdie, R.E. 2012.
1016   Subduction of the Chile ridge: upper mantle structure and flow. GSA Today (20) 9, 4-
1017   10. doi: 10.1130/GSATG61A.1.

1018

1019 SERNAGEOMIN 2002. Carta Geologica de Chile, N°75, Escala: 1,000,000, Hoja 3, Servicio
1020   Nacional de Geologia y Mineria, Subdireccion Nacional de Geologia, Chile.

1021

1022 Singer, B.S.; Ackert, R.P.; and Guillou, H. 2004. ^{40}Ar/^{39}Ar and K-Ar chronology of
1023   Pleistocene glaciations in Patagonia. Geological Society of America Bulletin 116, 434-450,
1024   doi: 10.1130/B25177.1

1025

1026 Singer, B.; Hildreth, W.; Vincze, Y. 2000. ^{40}Ar/^{39}Ar evidence for early deglaciation of the
1027   central Chilean Andes. Geophysical Research Letters 27, 1663-1666.

1028

1029 Stone, J.O. 2000. Air pressure and cosmogenic isotope production. Journal of Geophysical
1030   Research (105) 23, 753-759.

1031

1032 Sugden, D.E.; Hulton, N.R.J.; Purves, R.S. 2002. Modelling the inception of the Patagonian
1033   icesheet. Quaternary International 95-96, 55-64.

1034

1035   Turner, K.J.; Fogwill, C.J.; McCulloch, R.D.; Sugden, D.E. 2005. Deglaciation of the eastern

1036   flank of the North Patagonian Icefield and associated continental-scale lake diversions.

1037   Geogr. Ann., 87A(2), 363-374.

1038

1039   Wenzens, G. 2005. Glacier advances east of the Southern Andes between the Last Glacial

1040   Maximum and 5,000 BP compared with lake terraces of the endorrheic Lago Cardiel (49

1041   degrees S, Patagonia, Argentina). Zeitschrift Fr Geomorphologie 49, 433–454.

1042

1043   Wenzens, G. 1999. Fluctuations of outlet and valley glaciers in the Southern Andes

1044   (Argentina) during the past 13,000 years. Quaternary Research 51, 238-247.

1045

1046   Wu, P. 1997. Effect of viscosity structure on fault potential and stress orientations in eastern

1047   Canada. Geophysical Journal International 130, 365-382.

1048
1049   **Figure captions and tables**

1050

1051   **Table 1.** Minimum Cosmic Ray (CRE) ages calculated from in situ produced ^{10}Be

1052   concentrations within morphological markers. Location of samples (Fig. 2).

1053

1054   **Table 2.** Elevation and age for terraces along the General Carrera Lake between 72°50' and

1055   70°57' W. The data are graphically used at Fig. 14. A–Avellano; Al–Puerto Alarcon; DE–

1056   Dunas E; DW–Dunas W; EP–El Porvenir; FS–Fachinal; HW–Las Horquetas W; IB–Puerto

1057   Ibañez; LB–Lago Bertrand; LN—Lago Negro; Mu–Murta; Ma–Maitenes; PB–Punta Baja;

1058   PM–Perito Moreno; S–Sanchez. fan–fan delta sediment; N–north shore; S–south shore; stra–

1059   strandline; T0 to T4–Terraces 0 to 4; green–sample number; red–sample age (ka); black–

1060   strandline elevation (m); **bold**–terrace elevation (max); *italic*–terrace elevation (min). Note that

1061   age at the third column from the left is from Lago Negro (LN). Location of samples at Fig. 2.

1062

1063   **Figure 1.** Location of the studied area (glacial extent during the LGM from Hulton et al., 1994;

1064   Caldenius, 1932). Grey is icefield including the North (NPI) and the South (SPI) Patagonian

1065   icefields at Present time. Khaki and white arrows show the locus of Westerlies and maximum

1066   moisture during the LGM (i.e. Oxygen Isotope Stage 2) and at Present, respectively.

1067   Subduction of the active spreading center along the Chile ridge occurs at the Chile triple

1068   junction (Bourgois et al., 2000) inducing the Patagonia slab window to develop at depth

1069   beneath the South America plate. The red dash line shows the Patagonia slab window
1070   development at depth (Russo et al., 2012; Breitsprecher and Thorkelson, 2009; Bourgois and
1071   Michaud, 2002). Note that the General Carrera-Buenos Aires Lake area is located along the
1072   northern boundary of the Patagonia slab window at depth. CTJ–Chile Triple Junction; GCBA–
1073   General Carrera-Buenos Aires Lake; NPI–North Patagonian icefield; PSW–Patagonia slab
1074   window; SPI–South Patagonian icefield. Location of Fig. 2 is shown.

1075

1076   **Figure 2.** Location of sampling sites (ages, Table 1) along the GCBA Lake area. Note that the
1077   GCBA Lake outflows to the Pacific Ocean through the Rio Baker at Present. Two different
1078   outlet heads have been potentially active during the past 27 ka: the Rio Bayo to the Pacific, and
1079   the Rio Deseado (see Fig. 7 for location) to the Atlantic. Note that a short segment of the Rio
1080   Baker valley connects the Pueyrredon-Cochrane Lake (152 m at Present) to the GCBA Lake
1081   (201 m at Present. Location of Fig. 7, 9, 11, 12, and 13 is shown.

1082

1083   **Figure 3.** Terraces and strandlines along the GCBA Lake. A, B northern rim, from east to west:
1084   (A) T0 to T2 terraces at Pto Ingeniero Ibañez (location Fig. 2 and 7); (B) T0 to T2 terraces at
1085   Rio Avellano, (location Fig. 2). C to F southern rim from east to west: (C) Strandline at 226-
1086   230 m, east of Los Antiguos (Location, Fig. 2 and 7), Buenos Aires Lake (Argentina); (D) T1
1087   terrace at Rio El Salto (46°34'06"S-72°05'50"W, location Fig. 2), note the typical Gilbert
1088   signature of the T1 terrace and the ~102 m deep incision of the basement rock (see text for
1089   more details); (E) T1 and T2 terraces at Rio de Las Dunas (location Fig. 2 and 9); (F) T1 and
1090   T2 terraces and associated strandlines in an area located 4-5 km east of Pto Guadal (location
1091   Fig. 2).

1092

1093   **Figure 4.** Fluctuating lake level regression and strandline records. (A) Alluvial fan delta at the
1094   Rio El Cañal (location Fig.2) outflow. A sequence of tempestite barriers characterizes the
1095   frontal part of the delta. Behind the coarse pebble barrier topset fine layers is accumulating. (B)
1096   Bay located few km east of Pto Guadal (location Fig. 2) exhibiting three successive tempestite
1097   barriers. Difference in elevation from right to left is about 3.5 m evidencing that GCBA Lake is
1098   regressing at Present. (C) Major sequence of strandline regression at Rio Las Dunas outflow
1099   area (Location Fig. 2 and 9). Note the pervasive signature of regressive strandline along the T1
1100   terrace cliff (point Y3, see Fig. 10 and text for more details). Lake regression is continuous
1101   between 320 m and 201 m. Tempests during short phases of stable water level left a strandline
1102   imprint (point Y1, see Fig. 10 and text for more details). (D) A sequence of strandlines (point

1103   Y6, see Fig. 10) similar to that at points Y1 and Y3 was identified at more than 500 m elevation

1104   indicating that processes of lake regression worked during a long regressive phase leaving a

1105   pervasive imprint at various elevations between 527 m and 201 m across the major terraces.

1106

1107   **Figure 5.** Moraine boulder and drop-stones. (A) Sample 15 (location Fig. 2 and 7), moraine

1108   boulder at the crest of a frontal moraine damming the Rio Fenix Chico river. This moraine,

1109   younger than the Menucos till, has recorded the last ice re-advance to the east (see text for more

1110   details). (B) Sample 31 (location Fig. 2 and 9), drop-stone atop the T3 terrace, note figure on

1111   the right for scale. (C) Sample 39 (Fig. 2 and 13A for location), drop stone on lake sediment

1112   accumulation. (D) Sample 57 (location Fig. 2 and 9), at this site tens of big drop stones exist.

1113   See text for more details.

1114

1115   **Figure 6.** Chronology for moraine boulders, drop stones on terraces, and glacial polish surface

1116   for collected samples. Horizontal bars indicate $\pm 1\sigma$ uncertainties for ^{10}Be CRE ages (Table 1).

1117   The lower panel shows ages for the moraine samples (blue numbers: western Bertrand outlet;

1118   brown numbers: eastern Perito Moreno outlet). Also shown are ages for six of the youngest

1119   moraines east of General Carrera-Buenos Aires Lake, which includes the Menucos (M) and the

1120   Fenix (FI to FV) moraines from the youngest to the oldest –i.e. from west to east- (thick dash

1121   line, ages from Kaplan et al., 2011).

1122   The central panel shows ages for dropstones (black numbers) on terraces, sample 25 is from a

1123   glacial polish. Brown error bars show the recalculated ages for moraines described by Douglass

1124   et al. (2005) at Fachinal (location Fig. 2).

1125   The upper panel shows the GISP2 ice core temperature for the Northern Hemisphere (Alley,

1126   2000). The cold event at 8.2 kyr (Alley et al., 1997) and the Heinrich events H1 and H2 (Peck

1127   et al., 2007) are also shown. Note that the end of the Antarctic Cold Reversal (at 12.9 ka,

1128   Jomelli et al., 2014; Kaplan et al., 2011) coincides roughly with the estimated age of a

1129   significant increase of the *Nothofagus* southern beech pollen at 12.3 ka (Moreno et al., 2009).

1130

1131   **Figure 7.** Moraines at the Perito Moreno outlet area. From west to east –i.e. from the youngest

1132   to the oldest- it includes (Douglass et al., 2006; Kaplan et al., 2004; Singer et al., 2004; Ackert

1133   et al., 2003): the Menucos and Fenix I-V moraines (17.3 $\pm$ 0.6 to 25.7 $\pm$ 0.9 ka), the Moreno I

1134   and II moraines (~109-244 ka), the Moreno III-Deseado-Telken moraines (~244-1016 ka). Note

1135   that the Rio Fenix Grande branches the Rio Fenix Chico at Perito Moreno (392 m, elevation at

1136   the divide between Pacific and Atlantic) to feed the GCBA Lake. At Present, no connection

exists between the Rio Fenix Grande and the Rio Deseado. Bold number—location of samples 4, 15, 17, 23 and 69; thin line with barb—main strandlines; thick violet dash-line–dry valley network. Location of Fig. 8 is shown; map location (west of 71°W) on Fig. 2.

Figure 8. Two contrasting morphological signatures recording the evolution of the Buenos Aires Lake. Above ~ 415 ± 5 m (northeastward) the pervasive braided pattern of meander loops characterizes an evolving ice lobe margin. Below 415 ± 5 m (southwestward), parallel regressive strandlines document that the lake was free of ice. Note that the passage from one situation to the other exhibits a very sharp morphological signature suggesting a sharp ice retreat.

Figure 9. (A) Terraces along the Rio Los Maitenes. Note that sediment accumulated along a valley cutting across the T1 terrace (location at point X) evidencing a transgressive event occurring between T0 and T1. Location on Fig. 9B. (B) Terraces along the Rio de Las Dunas and Rio Las Horquetas-Los Maitenes. Five fan-delta terraces developed along these rivers, from the youngest to the oldest it includes: T0 (201-238 m); T1 (302-347 m); T2 (432-468 m); T3 (472-495 m); T4 (499-528 m). Dash line—strandline; bold number—location of samples 31, 57, 59, 61, 71, 73. Location on Fig. 2. Location of Fig. 9A and 10 is shown. See text for more details.

Figure 10. Pervasive strandline imprint at the Rio de Las Dunas area. Topsets and cliffs of fan-delta structures –i.e. T0 to T4 terraces– exhibit regularly spaced –i.e. every 2 to 3-5 m in elevation– notches associated with tempest. This is obvious along the cliff of terrace T1 at point Y3 (see also Fig. 4 C). The strandline network at point Y3 exhibits downslope prolongation along the bay area at points Y2 and Y1 (see also Fig. 4 C) down to the shoreline at Present. The pervasive strandline network exists across T2, T3 and T4 terraces at areas at points Y4, Y5, and Y6. Figure 4 D shows the area at point Y6. Lake regression shows a pervasive imprint throughout elevations from 527 to 201 m, across the major terraces. Location at Fig. 9.

Figure 11. Terrace development at Rio Müller. (A) Map showing the T0, T1, and T2 terraces. (B) Looking to the north from point L located at Fig. 11A. (C) Looking to the south from point M located at Fig. 11A. (D) A 94 m deep incision developed after the T1 terrace accumulation. See text for more details. Location at Fig. 2.

35

Figure 12. (A) The western outlet area of the General Carrera Lake. At Present, the GCBA Lake streams to the Pacific through the Lago Bertrand and the Rio Baker spillways. The location of Fig. 12 B, 12 C and 13 is shown. (B) Location of samples 45 and 49. (C) The outflow zone to the Rio Baker exhibits two moraines, the Inner moraine ridge has dammed the Lago Plomo, the Outer moraine has previously obstructed the Rio Baker discharge toward the Pacific Ocean. Note that strandline notches the older moraine (Fig. 12 B and 12 C). Location of samples 51, 53, 55 is shown. See text for more details.

Figure 13. (A) The Lago Negro outlet area. (B) Cross-section located at Fig. 13 A. (C) The basement rock extending west of the moraine (see Fig 13 B) shows strandline notches higher than the moraine. (D) The fan-delta sediment underlying the moraine ridge exhibits forsets dipping to the NE that documents drainage toward the General Carrera Lake.

Figure 14. Geomorphic markers and ages along the GCBA Lake. Note that: (1) ultimate ice retreat at Buenos Aires Lake dates back to the ACR (12.9-14.5 ka); (2) T2 to T4 terraces along the General Carrera Lake show local development; (3) as opposed, T0 and T1 extend along the General Carrera Lake throughout; (4) T1 is older than 10.9 ± 1.3 ka; (5) the elevation versus Longitude regression line (purple line) for T1 terraces shows an eastward tilt (discussion of this tectonic deformation will be developed in a coming paper); (6) a major transgression phase occurred at ~ 7.9 ± 2 ka. A–Avellano; Al–Puerto Alarcon; DE–Dunas E; DW–Dunas W; EP–El Porvenir; FS–Fachinal; HW–Las Horquetas W; IB–Puerto Ibañez; LB–Lago Bertrand; LN—Lago Negro; Mu–Murta; Ma–Maitenes; PB–Punta Baja; PM–Perito Moreno; S–Sanchez. T0 to T4–terraces.

Figure 15. Basic data (rounded values) for calculating glacial isostatic rebound since the last major cold event at 7.9 ± 1.1 ka. (A) Lago Bertrand outlet to the Pacific, (B) central area of the GCBA Lake —i.e. outlet of the Rio de Las Dunas area—, (C) Perito Moreno outlet at the divide between Pacific and Atlantic. Red dash line shows the lake level at 7.9 ± 1.1 ka. Blue dash line, range elevation for ice damming at 7.9 ± 1.1 ka. See text for more details.
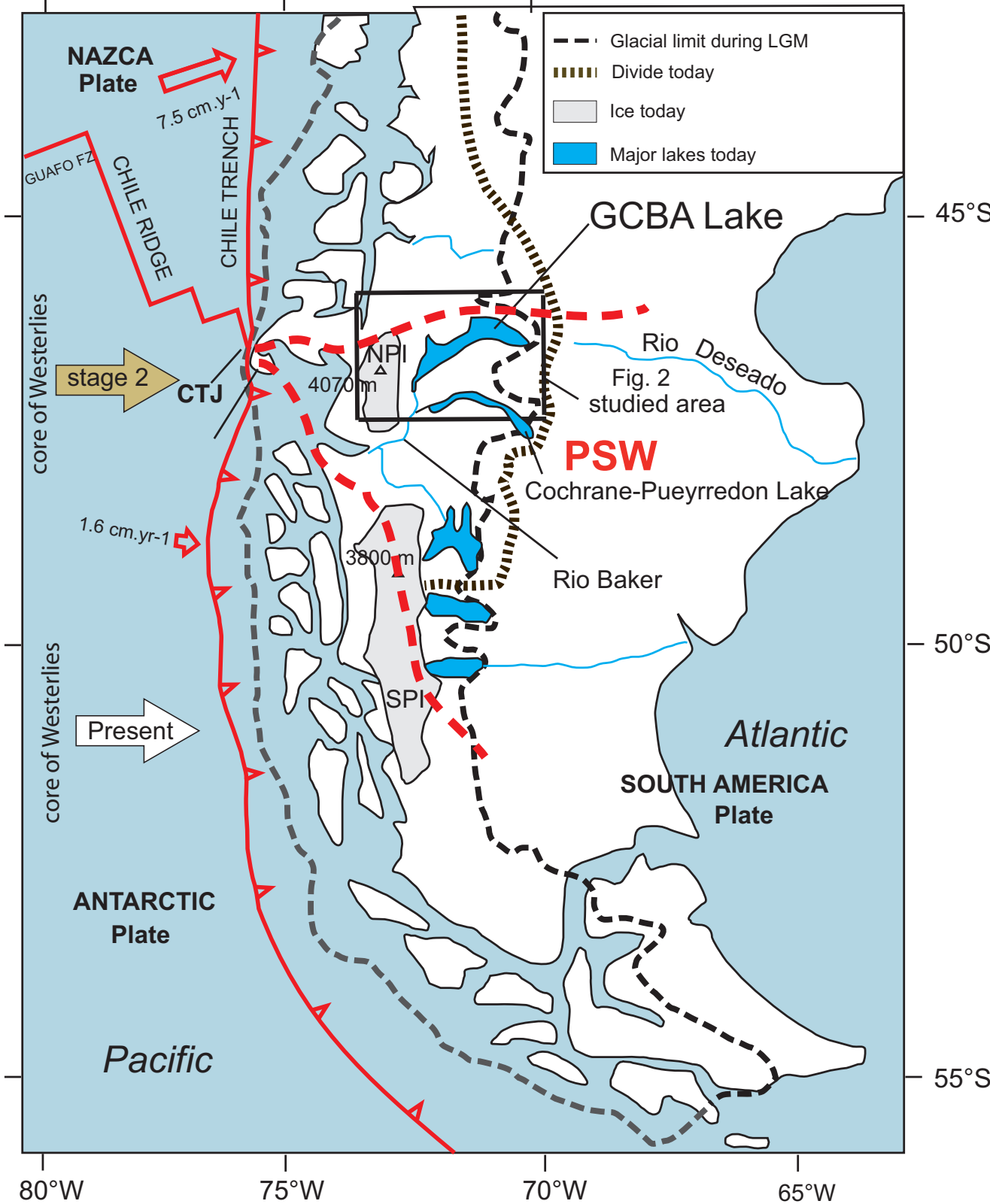
Pto Ingeniero Ibañez

Rio Fenix Grande

Bahia Murta

General Carrera Lake

Rio Avellano

Buenos Aires Lake

Perito Moreno

Rio Bayo

Rio Müller

GCBA   Lake

13

Rio Tranquilo

Fig. 11

Facinal

25

46°30'S

North

Rio Aviles

23

65

15

Patagonia

Rio El Cañal

Rio El Salto

Chile Chico

Rio Fenix Chico

69

59   31

57   71   61

CHILE

ARGENTINA

Los Antiguos

Fig. 7

45

73   Fig. 9

49

39

Lago Bertrand

55

Pto Guadal

51

53

47°S

Fig. 12 and 13

Icefield

Río Baker

CP Lake

Cochrane Lake

Pueyrredon Lake

47°30'S

73°W   72°30'W   72°W   71°30'W

13——13.9 ± 2.7 ka
15——20.5 ± 8.4 ka
23——34.2 ± 10.4 ka
25——13.3 ± 3.5 ka
31——16.5 ± 4.1 ka
39——14.4 ± 3.0 ka
45——17.5 ± 3.7 ka
49——20.0 ± 2.9 ka
51——23.8 ± 4.0 ka
53—— 8.6 ± 2.0 ka
55——18.9 ± 5.1 ka
57——18.5 ± 3.7 ka
59——15.0 ± 1.8 ka
61——15.2 ± 3.7 ka
65——19.3 ± 3.0 ka
69——20.2 ± 2.6 ka
71——18.8 ± 4.0 ka
73—— 9.9 ± 2.5 ka

Figure
Click here to download Figure: FIG 6 CHRONOLO.eps

Pto Ingeniero Ibañez

Strandline

MORENO I and II MORAINES
older than 109 ka

ice scar

4

Fig. 8

FENIX

MORENO III - DESEADO - TELKEN I-VI
MORAINES
younger than 1016 ka

Andean deformation

General Carrera Lake

MENUCOS

GCBA Lake

Chile Chico

MORAINES

392 m

Rio Deseado

Buenos Aires Lake

Los Antiguos

15

17

Rio Fenix Grande

23

69

Perito Moreno

lateral moraine
1116 m

Rio Jeinimeni

Rio Los Antiguos

Rio Fenix Chico

Cerro Volcan
109 ± 3 ka

Arroyo Page

Arroyo Page flow
760 ± 14 ka

basalt
Meseta de Lago
Buenos Aires

E-W trending dry valley network

landslide

Eastern limit of

71°30'W

71°W

70°30'W

46°20'S

46°45'S

0   (km)   25

Figure. Google Earth satellite image. Labels: 71°19'W, 46°22'S, 46°25'S, 71°09'W. "braided pattern of meander loops = ice lobe marginal drainage signature". "highest strandline at 12.9–14.5 ka". "415 ± 5 m". "FII 19.8 ± 0.6 ka". "FI 18.5 ± 0.8 ka". "M". "17.3 ± 0.6 ka". "FII". "FI". "N". "~3.5 km". "Buenos Aires Lake shoreline : 201 m". "parallel regressive strandlines = lake free of ice". "© 2013 InaV/Geosistemas SRL", "© 2013 Cnes/Spot Image", "Google earth", "Altitude 15.83 km".

A. looking to the south east

Rio Los Maitenes, Isla Macias, T4, T3, T2, T1, T0, X

B. GCBA Lake / General Carrera Lake, Isla Macias, Fig. 9A, 72°36'W, T0, T1, X, cliff, 31, Fig. 10, T2, T3, T4, 59, 57, 73, 71, Rio de Las Dunas, Rio Los Maitenes, Rio Las Horquetas, 46°45'S, 46°47'S, 72°47'W, 61, N, (km) 0–4

Figure
Click here to download Figure: FIG 11 RIO MÜLLER.eps

A
M
Rio Müller
T2
435 m
T2
X   T1   Y
319 m
T1
L
T0
basement
Image © 2014 DigitalGlobe
Image NASA
m
Date d

B   looking to the north from point L
basement
435 m
T2
319 m   376 m
T1

C   looking to the south from point M
basement
435 m T2
376 m
260 m

D
(m)   W
350
X   T1 Terrace   unconformity   Rio Müller incision   removed by erosion   E
Y
300
~ 94 m
250
225 m   basement rock
200

0   500   1000   (m)

B

El Martillo
309 m

46°50'S

strandline

General
Carrera Lake

45

fan delta sediment

OUTFLOW
201 m

500 m

302 m

moraine

250 m

263 m

46°51'S

Lago
Bertrand
72°49'W
500 m
72°48'W
49

C

72°52'W
Lago Bertrand
Outer moraine

72°50'W
Rio Bertrand
fan delta sediment
51
46°58'S

OUTFLOW

Inner
moraine

53

55

Rio
Baker

46°59'S

Lago Plomo

A

General Carrera
Lake

Fig. 12B

46°50'S

Lago
Bertrand

Lago Negro

Fig. 13

ice cap

Fig. 12C

Rio Bertrand

47°S

Lago Plomo

Rio Baker

73°W
72°45'W
72°30'W

A — Map showing General Carrera Lake, Lago Negro Lake, strandline (Fig. 13C), fan delta sediment, moraine, Fig. 13B, Fig. 13D, spot heights 341 m and 266 m, with contour lines at 250 m and 500 m. Coordinates 46°53'S, 46°54'S, 46°55'S, 72°48'W, 72°47'W. Scale bar 0–1 (km). North arrow. Label 39.

C — looking to the west; strandline; moraine 341 m.

D — looking to the east; NE dipping fan delta sediment; moraine.

B — Cross-section, W to E, elevation (m) 200–500. strandline, Fig. 13C; fan delta sediment Fig. 13D; moraine, Fig. 13C; metamorphic basement. Horizontal scale 500, 1000 (m).

Table

Sample number	Sample	Lat (°S)	long (°W)	Elevation (m)	Depth (cm)	Production at/g/yr
4	*M*	*46°24'19.4"*	*70°29'17.9"*	*644*	*1*	*7.391777778*
13	DS	46°31'22.4"	70°57'47.2"	451	2 to 5	6.32288889
15	M	46°32'31.8"	71°02'00.4"	392	2	6.01866667
17	*M*	*46°32'31.5"*	*71°00'43.0"*	*449*	*2*	*6.314666667*
23	M	46°34'52.7"	71°47'28.8"	1116	3	10.70533
25	GP	46°33'29.5"	71°52'02.4"	512	2 to 5	6.64355556
31	DS	46°46'51.1"	72°33'57.5"	494	1	6.63533333
39	DS	46°54'42.2"	72°47'27.4"	364	2	5.88711111
45	M	46°50'24.3"	72°48'19.6"	299	2	5.45955556
49	DS	46°51'01.6"	72°48'29.4"	334	2	5.63222222
51	M	46°58'34.2"	72°49'51.6"	360	3	5.78022222
53	DS	46°58'34.2"	72°50'00.1"	335	3	5.65688889
55	M	46°58'50.5"	72°51'42.0"	290	2 to 3	5.42666667
57	DS	46°48'39.9"	72°36'42.1"	501	2 to 3	6.53666667
59	DS	46°48'38.4"	72°37'19.1"	450	3	6.24888889
61	DS	46°44'45.9"	72°26'55.3"	520	2	6.64355556
65	M	46°39'50.2"	71°36'19.1"	572	2 to 3	6.93133333
69	M	46°35'23.9"	71°02'16.1"	441	2 to 3	6.17488889
71	DS	46°48'16.1"	72°35'19.8"	531	2 to 3	6.70933333
73	DS	46°48'22.0"	72°35'58.1"	521	2 to 3	6.65177778

The top of all samples were exposed at the surface
DS = Drop stone; M = Moraine; GP = Glacial polish

10Be	10Be error	Tmin	± 1s
at/g	at/g	(yr)	a
5,369,484	*228,487*	*913,185*	*38,859*
84,110	16,382	**13,940**	**2,715**
119,441	48,893	**20,463**	**8,377**
2,239,409	*274,129*	*401,656*	*49,167*
346 324	104 936	**34 164**	**10 352**
84,257	21,902	**13,292**	**3,455**
107,858	27,158	**16,464**	**4,145**
82,436	17,366	**14,414**	**3,036**
92,575	19,502	**17,457**	**3,678**
109,328	15,959	**20,002**	**2,920**
130,900	22,167	**23,774**	**4,026**
46,396	11,024	**8,576**	**2,038**
97,701	26,276	**18,869**	**5,075**
116,084	23,477	**18,472**	**3,736**
89,293	10,789	**14,977**	**1,810**
97,818	23,905	**15,170**	**3,707**
128,259	19,715	**19,258**	**2,960**
119,920	15,649	**20,201**	**2,636**
121,023	25,495	**18,766**	**3,953**
63,531	15,997	**9,914**	**2,496**

Table

Lake shore	W	N + S	N	S	N	S	S	S	S	N	S	N	N	E
Long W	72°50'	72°49' 72°47'	72°42' 72°40'	72°38' 72°35'	72°36' 72°34'	72°36' 72°33'	72°35' 72°34'	72°33' 72°31'	72°33'- 72°30'	72°31' 72°29'	72°14'- 72°12'	72°12' 72°08'	72°03' 71°56'	70°57'
	LB	PB+LN	Mu	EP	S	DW	DE	HW	Ma	Al	F	A	IB	PM
	fan/stra	stra/fan	fan	stra/fan	Fan	fan	fan	fan	fan	fan	Fan	fan	fan	stra
T4				57 19.1±3.9 **501**		73 10.1±2.5 **527** *504*	71 19.4±4.1 **528** *503*	**525** *501*	61 15.6±3.8 **520** *499*					13 14.3±2.8 **451**
T3						**492** *485*	31 17.0±4.3 **494** *472*	**495** *485*	**494** *481*					
T2				59 15.4±1.9 **452** *443*		**465** *433*	**468** *434*	**458** *441*	**445** *432*	**448** *413*		**413** *391*	**389** *370*	
T1	53 8.7±2.1 **349** *335*	39 14.8±3.1 **329** 364 *305*	**334** *302*	**339** *331*	**325** *309*	**347** *317*	**328** *316*	**330** *314*	**342** *302*	**329** *294*	**314** *293*	**326** *295*	**310** *281*	
T0	*201*	**232** *201*	**222** *201*	*201*	**228** *201*	**222** *201*	**222** *201*	**238** *201*	**238** *201*	**216** *201*	**225** *201*	**229** *201*	**226** *201*	